

1 **Eddy covariance data reveal that a small freshwater reservoir emits a substantial**
2 **amount of carbon dioxide and methane**

3 **Alexandria G. Hounshell^{1, †}, Brenda M. D'Acunha², Adrienne Breef-Pilz¹, Mark S.**
4 **Johnson^{2,3}, R. Quinn Thomas^{1,4}, Cayelan C. Carey¹**

5 ¹ Department of Biological Sciences, Virginia Tech, Blacksburg, VA, USA, ² Department of
6 Earth, Ocean, and Atmospheric Sciences, University of British Columbia, Vancouver, BC,
7 Canada, ³ Institute for Resources, Environment and Sustainability, University of British
8 Columbia, Vancouver, BC, Canada, ⁴ Department of Forest Resources and Environmental
9 Conservation, Virginia Tech, Blacksburg, VA, USA

10 Corresponding author: Alexandria G. Hounshell (alexgh@vt.edu)

11 † Current affiliation: National Centers for Coastal Ocean Science, National Oceanographic and
12 Atmospheric Administration, Beaufort, NC, 28516 alexandria.hounshell@noaa.gov

13 **Key Points:**

- 14 • We measured high annual CO₂ and CH₄ fluxes over 2 years from a small reservoir
- 15 • Fluxes were higher in the summer than winter, with statistically higher fluxes during
16 intermittent ice-on as compared to continuous ice-on
- 17 • Surface water temperature, thermocline depth, and dissolved organic matter
18 concentrations were correlated with reservoir fluxes

19 **Abstract**

20 Small freshwater reservoirs are ubiquitous and likely play an important role in global greenhouse
21 gas (GHG) budgets relative to their limited water surface area. However, constraining annual
22 GHG fluxes in small freshwater reservoirs is challenging given their footprint area and spatially
23 and temporally variable emissions. To quantify the GHG budget of a small (0.1 km²) reservoir,
24 we deployed an eddy covariance system in a small reservoir located in southwestern Virginia,
25 USA over two years to measure carbon dioxide (CO₂) and methane (CH₄) fluxes near-
26 continuously. Fluxes were coupled with *in situ* sensors measuring multiple environmental
27 parameters. Over both years, we found the reservoir to be a large source of CO₂ (633-731 g CO₂-
28 C m⁻² yr⁻¹) and CH₄ (1.02-1.29 g CH₄-C m⁻² yr⁻¹) to the atmosphere, with substantial sub-daily,
29 daily, weekly, and seasonal timescales of variability. For example, fluxes were substantially
30 greater during the summer thermally-stratified season as compared to the winter. In addition, we
31 observed significantly greater GHG fluxes during winter intermittent ice-on conditions as
32 compared to continuous ice-on conditions, suggesting GHG emissions from lakes and reservoirs
33 may increase with predicted decreases in winter ice-cover. Finally, we identified several key
34 environmental variables that may be driving reservoir GHG fluxes at multiple timescales,
35 including, surface water temperature and thermocline depth followed by fluorescent dissolved
36 organic matter. Overall, our novel year-round eddy covariance data from a small reservoir
37 indicate that these freshwater ecosystems likely contribute a substantial amount of CO₂ and CH₄
38 to global GHG budgets, relative to their surface area.

39

40 **Plain Language Summary**

41 Freshwater ecosystems release substantial amounts of greenhouse gases, especially carbon
42 dioxide and methane, to the atmosphere. Small waterbodies, such as lakes and reservoirs, are
43 common in the landscape and may release particularly high levels of greenhouse gases, though
44 their overall contribution remains unknown. The most common methods to date for estimating
45 greenhouse gas emissions from freshwaters typically involve only measuring concentrations
46 during the daytime on a handful of days throughout the year. Thus, there is a clear need for near-
47 continuous measurements of carbon dioxide and methane from small waterbodies throughout the
48 year on multiple timescales (hours to years). To do this, we measured fluxes of carbon dioxide

49 and methane from a small reservoir using eddy covariance over two years. We found this small
50 reservoir to be a large source of both carbon dioxide and methane to the atmosphere over two
51 years and found high variability in fluxes measured at short (sub-daily) to long (seasonal)
52 timescales. Overall, this study demonstrates the importance of small reservoirs as greenhouse gas
53 sources to the atmosphere and emphasizes the need for additional measurements to estimate their
54 contribution to global greenhouse gas budgets.

55

56 **1 Introduction**

57 Freshwater ecosystems play a disproportionately large role in global greenhouse gas
58 (GHG) budgets relative to their total water surface area, emitting more GHGs across all
59 freshwaters than are taken up by global terrestrial ecosystems (Bastviken et al. 2011; Cole et al.
60 2007; DelSontro et al. 2018; Tranvik et al. 2009). Despite their importance, however, the
61 contribution of inland waters, especially small ($<1 \text{ km}^2$) reservoirs, remains under-represented
62 within global carbon (C) and GHG budgets (Butman et al. 2018; Deemer and Holgerson, 2021;
63 Deemer et al. 2016; DelSontro et al. 2018). It is estimated that there are ~5.8 million lakes and
64 reservoirs in the contiguous U.S. (Winslow et al. 2014), of which approximately half (~2.6
65 million) are human-made reservoirs (Smith et al. 2002). Of these human-made reservoirs, small
66 reservoirs ($<1 \text{ km}^2$) compose $>71\%$ of reservoirs in the United States (National Inventory of
67 Dams, USACE 2021), indicating that these ecosystems are extremely common, with at least ~1.8
68 million small reservoirs in the conterminous U.S.

69 Despite their ubiquity, constraining annual GHG estimates in small freshwater reservoirs
70 is challenging given their small footprint area and heterogeneous GHG emissions (Loken et al.
71 2019; McClure et al. 2020; Podgrajsek et al. 2015). Short-term measurements indicate the
72 potential for these ecosystems to exhibit high, but patchy fluxes (Deemer and Holgerson, 2021;
73 DelSontro et al. 2018; McClure et al. 2018, 2020; Rosentreter et al. 2021), but to the best of our
74 knowledge, their annual emissions remain largely unknown. To date, most studies measuring
75 GHG emissions from freshwater lakes and reservoirs are based on snapshot measurements from
76 short-term floating chamber deployments or grab samples of dissolved GHGs, which are
77 extrapolated to broad spatial and temporal scales to estimate annual whole-ecosystem fluxes

78 (Bastviken et al. 2015; Klaus et al. 2019; Wik et al. 2016). While these approaches have
79 provided useful insights into general patterns of GHG cycling in freshwater ecosystems, they are
80 inherently limited in capturing the high spatial and temporal variability in freshwater GHG
81 fluxes (A.K. Baldocchi et al. 2020; Butman et al. 2018; Klaus et al. 2019; Rosentreter et al.
82 2021; Wik et al. 2016).

83 Eddy covariance (EC) systems are increasingly being deployed on lakes and reservoirs to
84 constrain sub-daily GHG fluxes over large spatial footprints, enabling the quantification of
85 whole-ecosystem GHG fluxes at multiple temporal scales (e.g., A.K. Baldocchi et al. 2020;
86 Golub et al. 2021; Eugster et al. 2011; Vesala et al. 2011; Waldo et al. 2021). EC systems are
87 used to determine the net exchange of carbon dioxide (CO₂), methane (CH₄), and/or other gases
88 at sub-hourly time scales via micrometeorology and *in situ* atmospheric trace gas concentrations
89 measured using infrared gas analyzers (A.K. Baldocchi et al. 2020; Golub et al. 2021; Vesala et
90 al. 2011). By collecting near-continuous, high frequency data (typically measured at 10-20 Hz
91 and reported as 30-minute means), EC systems allow GHG fluxes to be estimated at sub-daily to
92 annual timescales, improving our understanding of GHG flux temporal variability beyond
93 traditional discrete measurements (Golub et al. 2021; Reed et al. 2018; Vesala et al. 2011).
94 Additionally, EC systems often capture a larger spatial footprint compared to traditional discrete
95 measurements, as measured fluxes represent the average flux from the atmospherically-mixed
96 area upwind of the deployed EC system (Golub et al. 2021, Waldo et al. 2021). Thus, EC
97 systems can greatly increase the temporal resolution and spatial extent of measured fluxes in
98 lakes and reservoirs, with the caveat that important considerations and data filtering are needed
99 for EC systems in small waterbodies (Scholz et al. 2021). Specifically, a waterbody's small
100 surface area increases the likelihood of surrounding terrestrial vegetation impacting EC
101 measurements of aquatic fluxes and decreases the area available for a well-mixed, turbulent
102 footprint (Esters et al. 2020; Scholz et al. 2021; Vesala et al. 2011).

103 While the majority of reported freshwater EC studies have been conducted on short
104 timescales (days to months; e.g., Erkkiliä et al. 2018; Gorsky et al. 2021; Jammiet et al. 2015;
105 Podgrajsek et al. 2014, 2015; Vesala et al. 2006, 2011), longer-term studies measuring CO₂ or
106 CH₄ fluxes in lakes and reservoirs on annual timescales are becoming more common (e.g., A.K.
107 Baldocchi et al. 2020; Golub et al. 2021; Huotari et al. 2011; Jammiet et al. 2017; Liu et al. 2016;
108 Reed et al. 2018; Shao et al. 2015; Scholz et al. 2021; Taoka et al. 2020; Waldo et al. 2021). An

109 annual study conducted in Lake Erie, USA found this highly-eutrophic system was a small sink
110 of CO₂ during the summer productive season yet ultimately a CO₂ source on annual timescales
111 (Shao et al. 2015). Other studies have highlighted the importance of short (hourly to daily),
112 episodic events on annual CO₂ budgets, including the disproportionate effect of storms on annual
113 CO₂ emissions from a large subtropical reservoir (Liu et al. 2016), fall mixing in a large (40 km²)
114 temperate lake (Reed et al. 2018), and pulses of CH₄ following ice-off in a north temperate lake
115 (Gorsky et al. 2021). Studies conducted in the high northern latitudes during continuous ice-on
116 conditions in winter observed zero to very low greenhouse gas fluxes from frozen lakes due to
117 thick ice cover, which prevented the exchange of gasses across the air-water interface (e.g.,
118 Huotari et al. 2011; Jammot et al. 2017). In more temperate climates, other studies found low
119 and relatively consistent CO₂ fluxes during continuous or intermittent ice-covered winter periods
120 (A.K. Baldocchi et al. 2020; Reed et al. 2018). In addition to noted diel, seasonal, and episodic
121 variability in CO₂ fluxes, two annual studies recently found the sub-monthly timescale to be an
122 important timescale of variability, though the mechanism for this variability remains unknown
123 (A.K. Baldocchi et al. 2020; Golub et al. 2021). Altogether, despite the increase in studies using
124 EC systems to measure CO₂ and CH₄ fluxes from freshwaters, few studies to date have captured
125 *both* CO₂ and CH₄ fluxes on the annual scale, especially during winter.

126 Measuring annual-scale CO₂ and CH₄ fluxes is particularly important as GHG fluxes are
127 likely rapidly changing due to altered climate (Bartosiewicz et al. 2019; Beaulieu et al. 2019),
128 motivating several potential hypotheses for how different environmental drivers may alter fluxes.
129 Multiple environmental drivers sensitive to climate change likely affect GHG fluxes, though
130 annual-scale studies to test the effects of these drivers on fluxes across multiple timescales are
131 lacking. For example, increasing surface water temperatures and changes in precipitation and
132 nutrient loading are changing phytoplankton productivity and allochthonous C inputs to lakes
133 and reservoirs (Fowler et al. 2020; Hanson et al. 2015; Tranvik et al. 2009). For example,
134 changes in freshwater primary production and nutrient inputs to freshwater systems have been
135 directly linked to increases in CO₂ (DelSontro et al. 2018), as well as CH₄ emissions (Deemer
136 and Holgerson, 2021; DelSontro et al. 2018; McClure et al. 2020). Finally, increasing air
137 temperatures are leading to warmer winters and more intermittent and partial ice cover (Imrit and
138 Sharma, 2021; Sharma et al. 2021; Woolway et al. 2020), allowing for potentially greater
139 exchange of GHGs across the air-water interface, highlighting the need to understand the role of

140 ice in constraining GHG fluxes. All these examples emphasize the importance of measuring
141 near-continuous GHG fluxes on the annual scale along with key potential environmental drivers,
142 such as precipitation and freshwater inflows, surface water temperature, chlorophyll-*a*, dissolved
143 organic matter, and ice-on/ice-off as potential GHG drivers, as it is likely that some drivers may
144 have a greater effect at certain timescales than others.

145 Altogether, there is a clear need to measure annual-scale CH₄ and CO₂ fluxes from small
146 freshwater ecosystems, especially small reservoirs. While several studies have measured annual
147 CO₂ fluxes from freshwaters (e.g., A.K. Baldocchi et al. 2020; Golub et al. 2021; Huotari et al.
148 2011; Liu et al. 2016; Reed et al. 2018; Shao et al. 2015; Scholz et al. 2021), to the best of our
149 knowledge, only one freshwater study has measured *both* CH₄ and CO₂ fluxes on an annual
150 timescale (Jammet et al. 2017), while Taoka et al. (2020) and Waldo et al. (2021) measured only
151 CH₄ fluxes at the annual scale. Specifically, Waldo et al. (2021) used EC to measure annual CH₄
152 fluxes from a large (2.4 km²), highly-eutrophic temperate reservoir, measuring emissions up to
153 71.4 g CH₄ m⁻² yr⁻¹, which is in the top quarter of those reported from lakes and reservoirs to
154 date. In an Arctic lake, Jammet et al. (2017) used EC to measure low GHG fluxes during the
155 winter ice-covered period, followed by large CH₄ and CO₂ fluxes during spring-thaw, and
156 increasing ebullitive CH₄ fluxes during the ice-free season concurrent with small rates of CO₂
157 uptake during the summer due to photosynthesis. Aggregated across the full year, this Arctic lake
158 was a net source of both CH₄ and CO₂ to the atmosphere (Jammet et al. 2017). Across the
159 literature, most EC studies have focused on naturally-formed lakes, and all EC reservoir studies
160 of which we are aware (Eugster et al. 2011; Golub et al. 2021; Liu et al., 2016; Waldo et al.
161 2021) were conducted in large (>2.4 km²) reservoirs.

162 To better understand the GHG budgets of small reservoirs and the response of fluxes to
163 key environmental drivers, we deployed an EC system in a small (0.1 km²) freshwater reservoir
164 located in southwestern Virginia, USA for two years to measure *both* CO₂ and CH₄ fluxes near-
165 continuously. Flux measurements were coupled with *in situ* sensors measuring multiple
166 environmental parameters, including surface water temperature, dissolved oxygen, chlorophyll-*a*,
167 and fluorescent dissolved organic matter. Ultimately, we used the measured GHG fluxes and
168 environmental variables to answer the questions: 1) What is the annual phenology of CO₂ and
169 CH₄ fluxes in a small, eutrophic reservoir, including during the critical winter period?; and 2)
170 Which environmental variables best explain CO₂ and CH₄ variability at daily to monthly

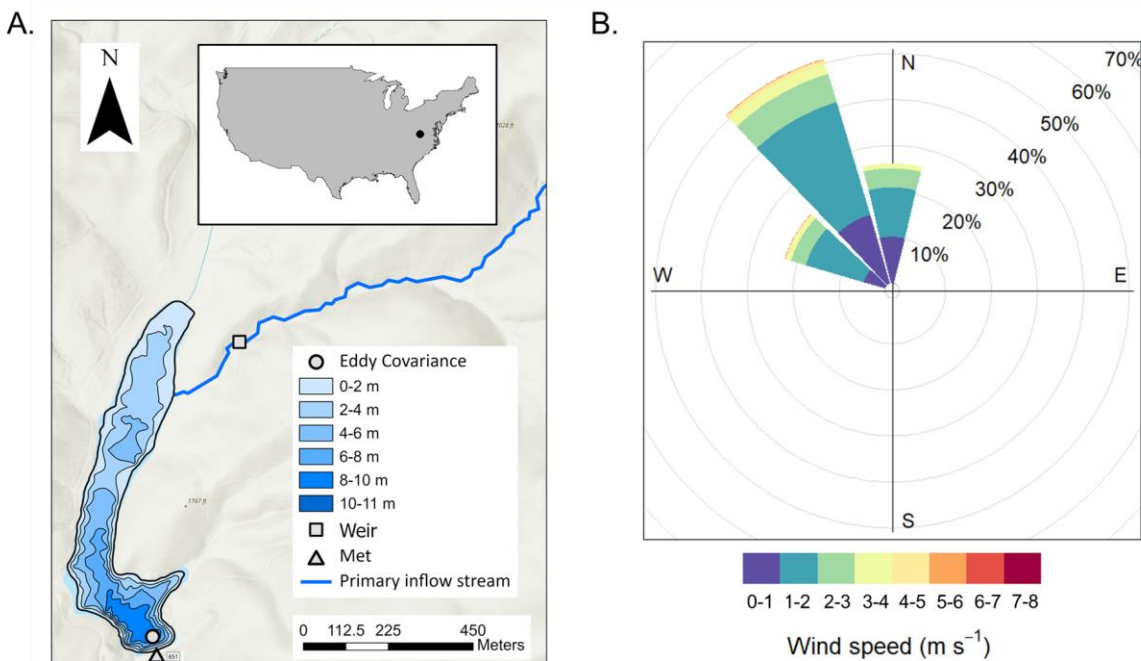
171 timescales? We expected CO₂ and CH₄ fluxes would be variable throughout the year, especially
172 during the summer months, when we expected larger GHG fluxes and marked diel patterns
173 following elevated primary production during the daylight hours. Conversely, during the winter
174 months, we expected relatively low fluxes due to suppressed biological activity and potential ice-
175 cover. Following these expectations, we predicted temperature would be an important
176 environmental predictor positively-related to both CO₂ and CH₄, while chlorophyll-*a* would
177 likely be an important environmental predictor positively related to CO₂ fluxes on multiple
178 timescales.

179

180 **2 Materials and Methods**

181 2.1 Site description

182 Falling Creek Reservoir (FCR) is a small, eutrophic reservoir located in Vinton, Virginia,
183 USA constructed in 1898 (Fig. 1; 37.303°N, 79.837°W; Gerling et al. 2016; Howard et al. 2021).
184 The reservoir is located in a valley at 520 m above sea level. Hills on either side of the reservoir
185 have a maximum elevation of 615 m (east) and 740 m (west) above sea level. The reservoir and
186 surrounding forested watershed are owned and operated by the Western Virginia Water
187 Authority (WVWA) as a primary drinking water source (Gerling et al. 2016). FCR has a surface
188 area of 0.119 km² and a maximum depth of 9.3 m (McClure et al. 2018). The reservoir is
189 dimictic and thermally stratified from April to October (McClure et al. 2018). During the
190 study period, water was not extracted for drinking water treatment and remained at a constant
191 full-pond level. The water residence time during the study period ranged from 21 to 635 d, with a
192 median of 247 d (Fig. S1; calculated using the methods of Gerling et al. 2014). Since the
193 reservoir remained at full pond, we assumed incoming discharge from the primary inflow was
194 equal to outflowing discharge during the two-year study period.



195
 196 **Figure 1.** A. Map of Falling Creek Reservoir (FCR) located in Vinton, Virginia, USA (map
 197 inset) showing location of the eddy covariance system, the weir located on the primary
 198 freshwater inflow, and the meteorological station located on the dam. B. Wind rose showing the
 199 dominant wind direction and wind speed (m s^{-1}) of greenhouse gas fluxes retained for analysis.
 200 The cumulative footprint distribution for the study period is shown in the supplementary
 201 information (Fig. S2).

202 2.2 Data collection and overview

203 We used an EC system deployed near the dam on an existing metal platform extending
 204 into the reservoir to measure CO_2 and CH_4 fluxes between the water surface and the atmosphere
 205 from 1 May 2020 to 30 April 2022 (details below; Carey et al. 2022a). To complement the EC
 206 measured fluxes, we also calculated CO_2 and CH_4 diffusive gas fluxes using dissolved CO_2 and
 207 CH_4 discrete grab samples collected during daylight hours (between ~08:00 to 13:00) weekly to
 208 monthly from the water's surface at the deepest site of the reservoir, located near the dam,
 209 throughout the 2-year study period (details below; Carey et al. 2022b). The EC system was co-
 210 located near the reservoir dam to take advantage of the existing limnological and meteorological
 211 suite of instruments already deployed at this location as well as existing electrical power and
 212 infrastructure for EC deployment.

213 In addition to the EC and diffusive fluxes, we also collected meteorological and
 214 environmental data. Briefly, a Campbell Scientific (Logan, Utah, USA) research-grade

215 meteorological station measured air temperature; relative humidity; air pressure; wind speed and
216 direction; upwelling and downwelling shortwave and longwave radiation; total rainfall;
217 photosynthetically-active radiation (PAR); and albedo every minute at the reservoir dam (sensor
218 information provided by Carey et al. 2022c). At the reservoir's deepest site, we collected 10-
219 minute water temperature measurements every 1 m from the surface (0.1 m) to just above the
220 sediments (9 m) using a thermistor string. Thermistor data were used to calculate the difference
221 in temperature between 0.1 m and 9.0 m (Diff. Temp) and daily buoyancy frequency (N^2), two
222 metrics of thermal stratification, as well as thermocline depth throughout the study period (May
223 2020 to April 2022) using the LakeAnalyzer package in R (Winslow et al. 2016a). Fall turnover
224 was defined as the first day in autumn when the temperature at 1 m was $<1^\circ\text{C}$ of the temperature
225 measured at 8 m (1 November 2020 and 3 November 2021; McClure et al. 2018). Spring mixing
226 was harder to identify due to intermittent ice-on in 2021 and frequent mixing during the winter
227 period, but we defined spring mixing as the first day in spring after complete ice-off when the
228 temperature at 1 m was $<1^\circ\text{C}$ of the temperature measured at 8 m (26 February 2021 and 10
229 February 2022). For 2022, spring mixing occurred on the same day as complete ice-off. Ice cover
230 was determined by the presence of inverse stratification coupled with higher albedo and verified
231 by visual observation, described by Carey and Breef-Pilz (2022).

232 Water column temperature data complemented 10-minute measurements of dissolved
233 oxygen (DO) percent saturation, chlorophyll-*a* (Chl-*a*, $\mu\text{g L}^{-1}$), and fluorescent dissolved organic
234 matter (fDOM, relative fluorescent units, RFU) measured using an EXO2 sonde (YSI, Yellow
235 Springs, Ohio, USA) deployed at 1.6 m (Carey et al. 2022d), which is the depth historically used
236 for water extraction when the reservoir is in-use (Howard et al. 2021). The EXO2 sonde was
237 removed from the reservoir on 2 December 2020 for annual sensor maintenance and re-deployed
238 on 27 December 2020. Finally, we measured stream inflow every 15 minutes on the primary
239 inflowing stream to the reservoir via a gaged v-notch weir fitted with a Campbell Scientific
240 CS451 pressure transducer (Campbell Scientific, Logan, Utah, USA), which was used to
241 calculate the 15-minute flow rate following Carey et al. (2022e). The weir was breached on 20
242 July 2020 and repaired on 24 August 2020, resulting in no flow data during this interval.

243 2.3 Eddy covariance flux measurements

244 An EC system was deployed above the water surface over the deepest portion of the
245 reservoir from 1 May 2020 to 30 April 2022. The EC instrumentation was installed 2.9 m over
246 the reservoir's surface on a permanent metal platform that extends ~45 m from the dam. As noted
247 above, the reservoir was maintained at full pond, resulting in a consistent height of the EC
248 system over the water's surface during the study period. The placement of the EC sensors at 2.9
249 m above the water surface reflects a balance between ensuring adequate frequency responses to
250 capture eddies (Burba and Anderson, 2010) and capturing a flux footprint that represents the area
251 of interest. This height resulted in a flux footprint that was generally well matched to the
252 reservoir (Fig. S2).

253 The EC system included an ultrasonic anemometer to measure 3D wind speed and
254 direction (CSAT3, Campbell Scientific), an open-path infrared gas analyzer for measuring CH₄
255 concentration (LI-7700, LiCor Biosciences, Lincoln, Nebraska, USA), and an enclosed-path
256 infrared gas analyzer for measuring CO₂ and water vapor concentrations (LI-7200, LiCor
257 Biosciences), all recorded at 10 Hz by a data logger (LI-7550, LiCor Biosciences). On 10 August
258 2020, the data logger was removed for maintenance and re-deployed on 2 September 2020.
259 Additionally, a thermocouple on the CO₂ sensor (LI-7200) was inoperable starting on 5 April
260 2021 and was repaired on 26 April 2021.

261 The raw 10-Hz data were first processed into 30-minute fluxes using the EddyPro v.7.0.6
262 software (LiCor Biosciences 2019). Fluxes were calculated following standard methods in
263 EddyPro v.7.0.6 (LiCor Biosciences 2019), which included spike detection and removal (Vickers
264 and Mahrt, 1997), a double rotation for tilt correction (Lee et al. 2005), linear detrending (Gash
265 and Culf, 1996), time lag compensation, and spectral corrections for high and low-pass filtering
266 effects following Moncrieff et al. (2004) and Moncrieff et al. (1997), respectively. In addition,
267 CH₄ molar density was corrected to account for air density fluctuations and spectroscopic effects
268 of temperature, pressure and water vapor (McDermitt et al. 2011; Webb et al. 1980). This
269 correction was not needed for CO₂, as fluxes were estimated using mixing ratios instead of
270 densities (Burba et al. 2012).

271 Following initial flux calculations and processing in EddyPro, we conducted additional
272 data processing following standard best practices, including: 1) removing wind directions which
273 originated outside of the reservoir (80-250°; Fig. 1); 2) removing extreme flux values (CO₂
274 fluxes $\geq |100| \mu\text{mol C m}^{-2} \text{ s}^{-1}$; CH₄ fluxes $\geq |0.25| \mu\text{mol C m}^{-2} \text{ s}^{-1}$); 3) removing CH₄ fluxes when
275 signal strength <20%; 4) removing CO₂ and CH₄ fluxes when they did not pass the test for
276 stationarity or developed turbulent conditions (QC, quality control level 2 per Mauder and
277 Foken, 2006), in addition to when the latent heat (LE) or sensible heat flux (H) had QC level <2;
278 5) removing open-path CH₄ fluxes during periods of rainfall, which was determined based on the
279 rain gauge deployed at the dam; 6) removing additional periods of low turbulence friction
280 velocity (u^*), as described below; and 7) removing data that corresponded to flux footprints that
281 extended significantly beyond the reservoir. We used REddyProc (Wutzler et al. 2021) to
282 determine the u^* threshold for sufficiently turbulent conditions and removed any fluxes where u^*
283 was $< 0.075 \text{ m s}^{-1}$. To account for the uncertainty of estimating the u^* threshold, we used
284 bootstrapping to estimate the distribution of u^* thresholds, and obtained the 5th, 50th and 95th
285 percentiles of this distribution (0.070, 0.075, and 0.163 m s^{-1} , respectively; Wutzler et al., 2018).

286 The final filtering step consisted of removing fluxes that extended beyond the reservoir.
287 To do that, flux footprints were modeled for each half-hour using a simple, two-dimensional
288 parameterization developed by Kljun et al. (2015) (Fig. S2). This model builds on the
289 Lagrangian stochastic particle dispersion model (Kljun et al. 2002), and provides information on
290 the extent, width, and shape of the footprint. All the variables needed for the model were
291 obtained directly from the dataset described above or calculated following Kljun et al. (2015).
292 Fluxes were excluded when the along-wind distance providing 90% cumulative contribution to
293 turbulent fluxes was outside the reservoir, based on the footprint analysis. We chose to use this
294 filtering threshold given the challenges of modeling footprints in small reservoirs; consequently,
295 our fluxes are likely conservative. All post-processing analyses were conducted using R
296 statistical software (v.4.0.3). Code for post-processing and all EC data can be found in the
297 Environmental Data Initiative (EDI) repository (Carey et al. 2022a).

298 Overall, EC measurements captured 23% and 19% of total CO₂ and CH₄ fluxes,
299 respectively, over two years from FCR (Table S1), which is similar to previously-reported
300 deployments of EC systems at lakes and reservoirs (e.g., Golub et al. 2021; Reed et al. 2018;

301 Waldo et al. 2021). The percentage of available data was relatively consistent across half-hourly
302 periods (from 00:00 to 23:30), ranging from 14%-34% of data availability for CO₂ for 22:00 and
303 12:30 half-hourly periods, respectively, and 11%-32% for CH₄ (22:00 and 12:30 half-hourly
304 periods, respectively; Fig. S3). We note that during the day, the dominant wind direction was
305 outside the reservoir footprint, while the dominant wind direction was largely along the reservoir
306 at night (Fig. S4). This pattern resulted in a high percentage of daytime fluxes removed due to
307 wind direction, but overall, we observed a roughly equal contribution of day and night fluxes
308 following all flux removal processes (i.e., flux filtering due to low u*). Data availability after
309 filtering was also relatively consistent throughout seasons and between years, ensuring even
310 representation of measured fluxes throughout the year (Fig. S5). We do note low data availability
311 (<10%) for both CO₂ and CH₄ fluxes during August 2020, due to instrument maintenance, and
312 for CH₄ during December 2020 and February 2021 due to issues with instrument power stability.

313 2.4 Diffusive flux measurements

314 We estimated discrete diffusive fluxes from FCR using dissolved CO₂ and CH₄ samples
315 (Carey et al. 2022b) collected at the surface of the reservoir to compare with EC fluxes. Surface
316 water samples were collected at 0.1 m depth using a 4-L Van Dorn sampler (Wildlife Supply
317 Co., Yulee, Florida, USA) adjacent to the EC sensors (Fig. 1). Replicate (n=2) water samples
318 were collected via a Van Dorn sampler into 20-mL serum vials without headspace, immediately
319 capped, and then stored on ice until analysis within 24 hours. Prior to sample analysis, a small
320 amount of water was removed from each sample and replaced with a neutral gas (helium gas).
321 Samples were analyzed following Carey et al. (2022b) on a Shimadzu Nexis GC-2030 Gas
322 Chromatograph (Kyoto, Japan) with a Flame Ionization Detector (GC-FID) and Thermal
323 Conductivity Detector (TCD).

324 The measured surface samples were used to calculate CO₂ and CH₄ diffusive fluxes from
325 the surface of FCR into the atmosphere on each day of sample collection following the equation:

$$326 \quad Flux = k * (C_{water} - C_{eq}) \quad Eq. 1$$

327 where k is the temperature-corrected gas transfer velocity (m d⁻¹) for the gas species (CO₂ or
328 CH₄, respectively), and (C_{water} - C_{eq}) is the dissolved gas concentration in excess of

329 atmospheric concentrations (Cole and Caraco, 1998; Wanninkhof et al. 2009). C_{water} is the
330 concentration (mass volume⁻¹) of CO₂ or CH₄ at the reservoir surface (0.1 m), and C_{eq} is the
331 concentration of dissolved gas at equilibrium with the EC-measured atmospheric concentration
332 of CO₂ or CH₄. The GHG flux value was calculated separately for each of the two dissolved
333 GHG sample replicates collected at each time point using the seven k models included in the
334 LakeMetabolizer package in R (Cole and Caraco, 1998; Crusius and Wanninkhof 2003;
335 Heiskanen et al. 2014; MacIntyre et al. 2010; Read et al. 2012; Soloviev et al. 2007; Vachon and
336 Prairie, 2013; Winslow et al. 2016b, 2016c). We report the mean and standard deviation from the
337 n=14 replicate-model k determinations to account for uncertainty introduced through various k
338 estimations. We feel this approach offers the best representation of potential diffusive flux values
339 that can be directly compared to fluxes measured by EC (Erkkilä et al. 2018; Schubert et al.
340 2012).

341 2.5 Statistical analyses

342 To assess the phenology of fluxes (CO₂ and CH₄), we analyzed the mean and standard
343 deviation (± 1 S.D.) of measured EC fluxes at half-hourly, daily, weekly, and monthly time scales
344 through the study period. For both EC and discrete diffusive fluxes, negative fluxes correspond
345 to fluxes into the reservoir (i.e., uptake) while positive fluxes are out of the reservoir (i.e., release
346 to the atmosphere).

347 To assess diel variation in GHG fluxes, we compared median measured EC fluxes during
348 the day (11:00 to 13:00) and night (23:00 to 01:00) throughout the study period. As data were not
349 normally distributed, we used paired Wilcoxon signed-rank tests to assess statistical significance
350 of paired day-night fluxes ($\alpha = 0.05$). Additionally, we compared dawn (05:00 to 07:00) and
351 dusk (17:00 to 19:00) median EC measured fluxes using the same methods.

352 Ice coverage at FCR is episodic and ephemeral, encompassing longer ice-covered periods
353 as well as shorter-duration ice-covered periods when ice may be present during portions of
354 sequential days or with partial coverage of the reservoir's surface, which we refer to as
355 intermittent ice-on periods. To explore the role of variable winter ice cover on CO₂ and CH₄
356 fluxes, we analyzed mean half-hourly fluxes (± 1 S.D.) from 10 January to 10 February for both
357 2021 and 2022, which encompassed a period of intermittent (2021) and continuous (2022) ice-on

358 (following Carey and Breef-Pilz 2022; Table S2). We used Mann-Whitney-Wilcoxon tests to
359 determine statistically-significant differences ($\alpha = 0.05$) between the median half-hourly fluxes
360 measured during intermittent and continuous ice-on periods.

361 Finally, we calculated the net annual flux balance for CO₂ and CH₄ using both measured
362 and gap-filled half-hourly EC data. Briefly, after filtering, half-hourly fluxes were gap-filled in
363 REddyProc using the marginal distribution sampling method (MDS), which uses the correlation
364 of measured fluxes with environmental driver variables, namely, radiation, temperature, and
365 vapor pressure deficit (VPD) to estimate fluxes during the missing time periods (Wutzler et al.
366 2018). Prior to MDS, we used the meteorological data measured at the dam to gap-fill any
367 missing wind speed, direction, temperature, and relative humidity in the EC dataset (Table S3).
368 Overlapping data show that all meteorological variables were tightly correlated between the EC
369 system and the adjacent meteorological station (Pearson's rho=0.81-0.98; Table S3). Gap-filling
370 was performed for each of the u* scenarios, providing information about the uncertainty that
371 might be introduced to the data by choosing a u* threshold. Measured and gap-filled fluxes were
372 summed across each year (01 May - 30 April). The standard deviation (± 1 S.D.) was calculated
373 for both the measured and gap-filled data using the different u* scenarios.

374 2.6 Time series analysis

375 To identify key environmental predictors and test mechanistic relationships between
376 observed mean daily, weekly, and monthly measured CO₂ and CH₄ fluxes and environmental
377 variables, we developed separate autoregressive integrated moving average (ARIMA) models for
378 each timescale. ARIMA models are used to identify key environmental predictors while
379 accounting for temporal autocorrelation (Hyndman and Athanasopoulos, 2018). We selected
380 several potential, in-reservoir, environmental predictors, including: surface water temperature
381 (Temp, 0.1 m, °C); the difference between surface (0.1 m) and bottom (9 m) water temperatures
382 (Diff. Temp); buoyancy frequency (N²); thermocline depth (TD); DO percent saturation (DO
383 sat); Chl-*a*; fDOM; and discharge (Inflow) measured at the primary inflow to FCR (Fig. S6, S7).
384 We chose to focus on limnological environmental variables to help identify potential drivers of
385 GHG fluxes, following our predictions. Prior to ARIMA modeling, we conducted pairwise
386 Spearman correlations on all predictor variables (aggregated to each time scale) and removed

387 collinear variables (Pearson's $\rho \geq 0.7$) that were the least correlated with fluxes. N^2 and Diff.
388 Temp were removed for all time scales due to their strong correlation with surface water
389 temperature (Table S4). Response and predictor variables were checked for skewness,
390 transformed if appropriate, and normalized (z-scores) prior to model fitting (Hounshell et al.
391 2022).

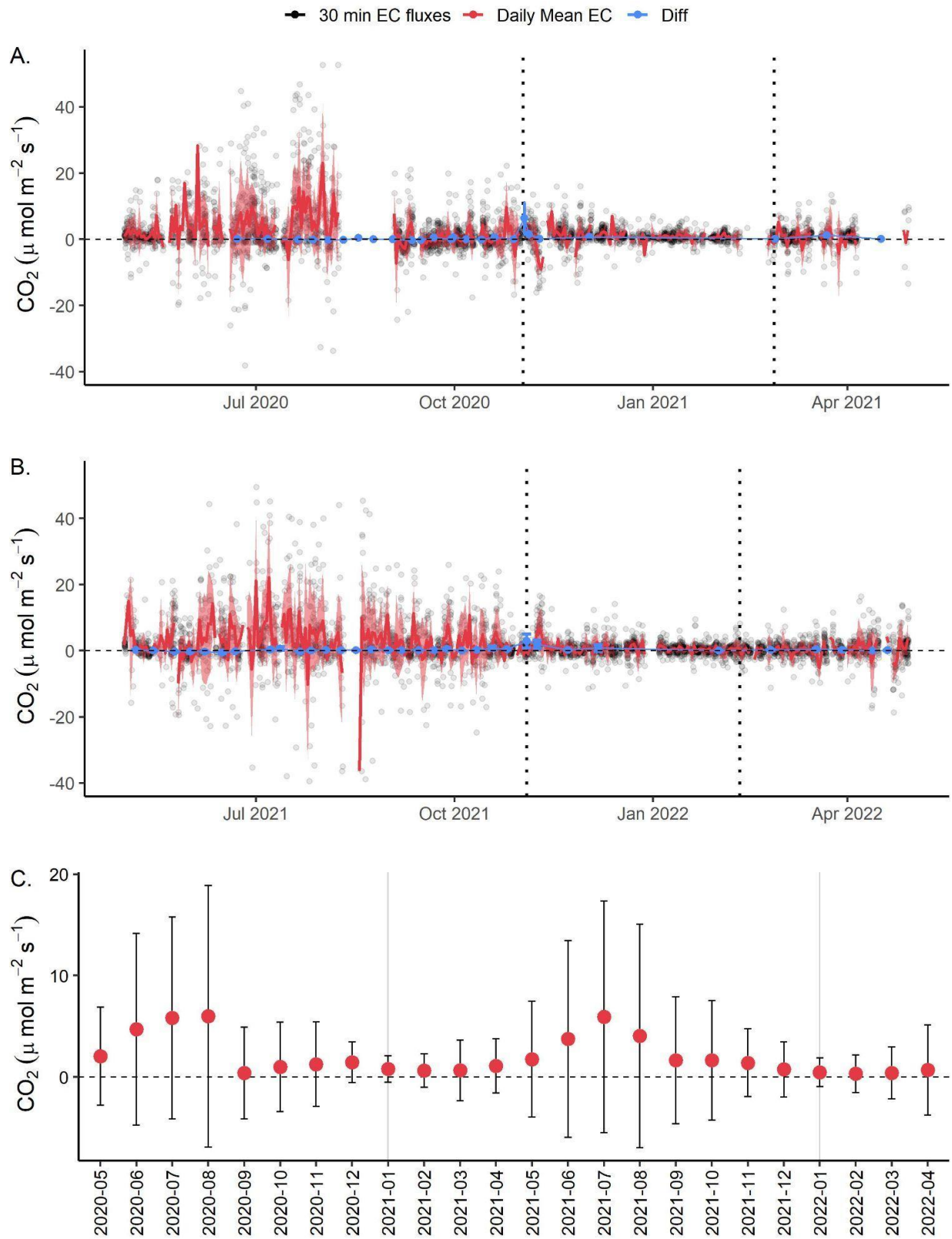
392 We used a model selection algorithm (Lofton et al. 2022) to identify the importance of
393 environmental predictor variables at each time scale. The algorithm was based on the auto.arima
394 function in the forecast package in R (Hyndman and Khandakar, 2008; Hyndman et al. 2021)
395 which compared fitted models to a global model (all possible predictors) and a null persistence
396 model with just one autoregressive term (AR(1)). We selected the environmental model with the
397 lowest corrected Akaike information criterion (AICc), as well as models within 2 AICc units
398 (Burnham and Anderson, 2002). Models were limited to include one autoregressive term
399 (Hounshell et al. 2022).

400

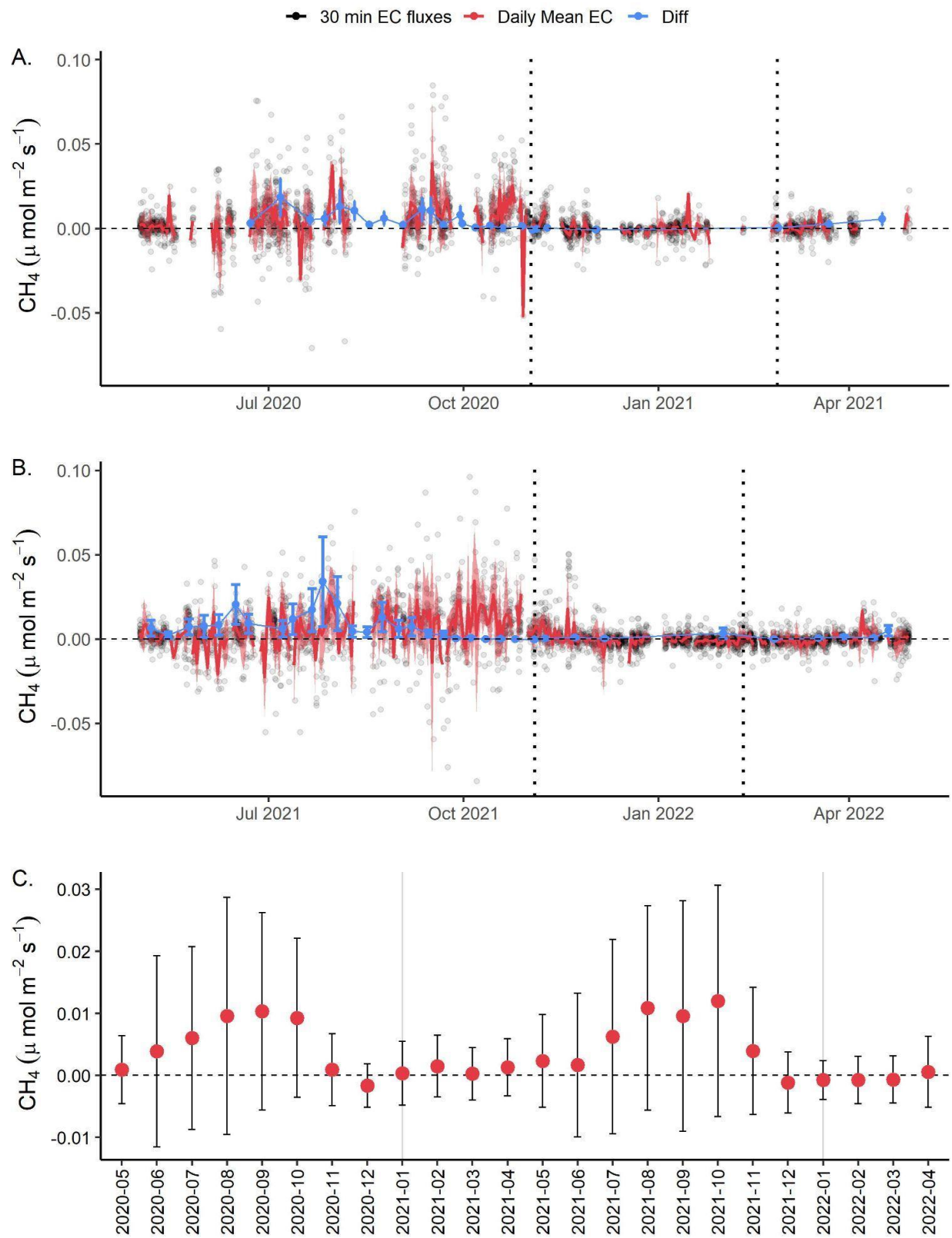
401 **3 Results**

402 3.1 Phenology of CO₂ and CH₄ fluxes

403 High-frequency EC data show that FCR was generally a net source of both CO₂ and CH₄
404 to the atmosphere across multiple timescales (Figs. 2, 3, S7; Tables S5). Overall, measured CO₂
405 fluxes ranged from -39.46 to 52.67 $\mu\text{mol m}^{-2} \text{s}^{-1}$ with a mean flux of $1.86 \pm 6.21 \mu\text{mol m}^{-2} \text{s}^{-1}$ (± 1
406 S.D.) aggregated over the entire 2-year study period. Measured CH₄ fluxes ranged from -0.084 to
407 0.096 $\mu\text{mol m}^{-2} \text{s}^{-1}$, with a mean CH₄ flux of $0.003 \pm 0.011 \mu\text{mol m}^{-2} \text{s}^{-1}$ over the study period
408 (Fig. 2, 3, S8; Table S5).

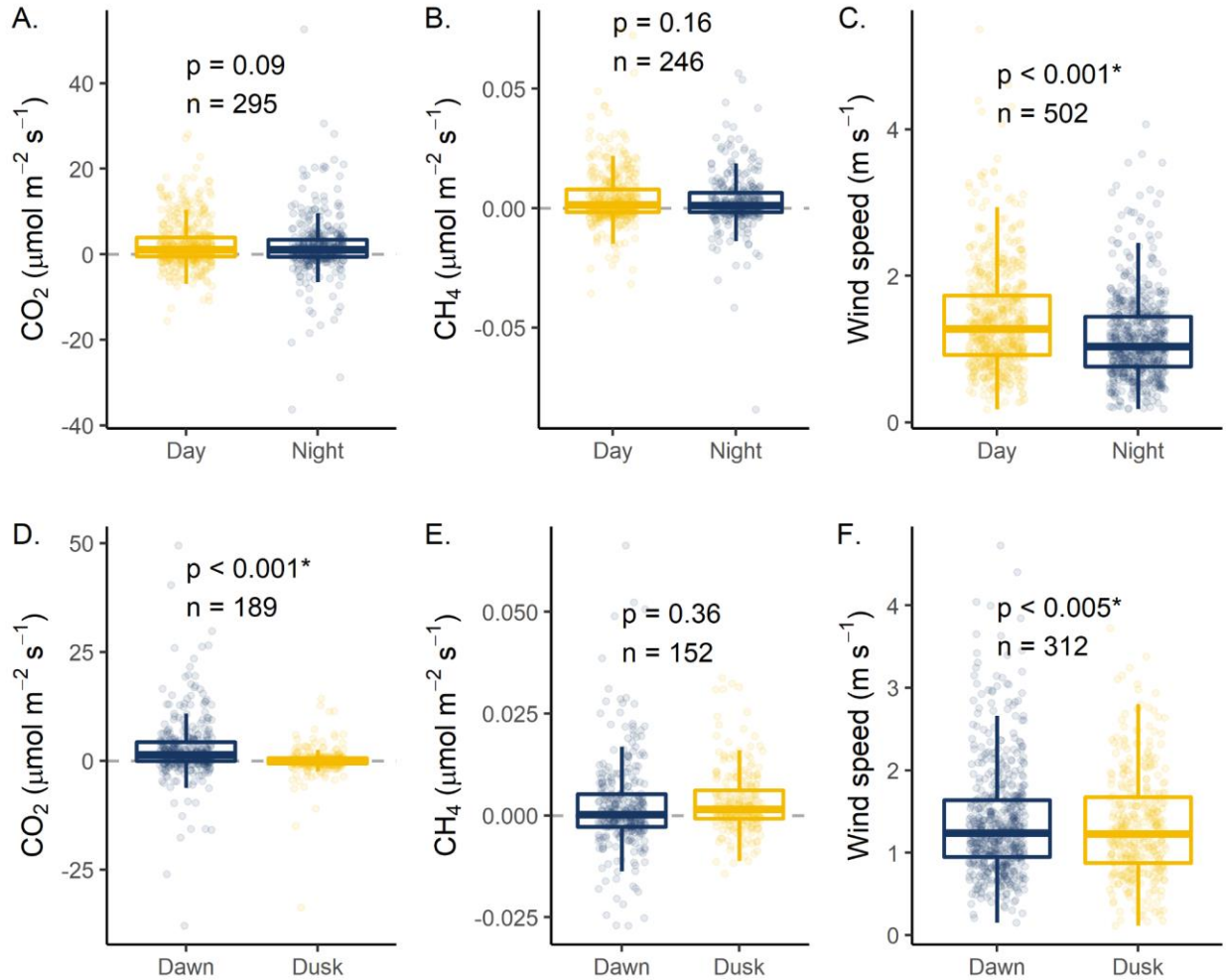


410 **Figure 2.** Daily mean carbon dioxide fluxes (CO_2 , $\mu\text{mol m}^{-2} \text{s}^{-1}$) for A. May 2020 to April 2021
411 (Year 1) and B. May 2021 to April 2022 (Year 2) measured using eddy covariance (Daily Mean
412 EC, red) and calculated discrete diffusive fluxes (Diff, blue) using the mean and standard
413 deviation of two replicate samples and seven gas transfer coefficient models (k ; Winslow et al.
414 2016b). Grey dots represent measured half-hourly fluxes from the EC. The dark red line
415 represents daily mean fluxes. The shaded red area represents ± 1 standard deviation of the daily
416 30-minute fluxes using measured EC fluxes. The vertical dotted line indicates the onset of
417 reservoir fall and spring mixing, respectively. C. Mean monthly CO_2 fluxes ($\mu\text{mol m}^{-2} \text{s}^{-1}$)
418 aggregated from measured EC data. The error bars correspond to ± 1 S.D. of aggregated fluxes
419 for both measured and gap-filled EC values. The horizontal dashed line indicates zero fluxes.



421 **Figure 3.** Daily mean methane fluxes (CH_4 , $\mu\text{mol m}^{-2} \text{s}^{-1}$) for A. May 2020 to April 2021 (Year
422 1) and B. May 2021 to April 2022 (Year 2) measured using eddy covariance (Daily Mean EC,
423 red) and calculated discrete diffusive fluxes (Diff, blue) using the mean and standard deviation of
424 two replicate samples and seven gas transfer coefficient models (k ; Winslow et al. 2016b). Grey
425 dots represent measured half-hourly fluxes from the EC. The dark red line represents daily mean
426 fluxes. The shaded red area represents ± 1 standard deviation of the daily 30-minute fluxes. The
427 vertical dotted line indicates the onset of reservoir fall and spring mixing for each year,
428 respectively. C. Mean monthly CH_4 fluxes ($\mu\text{mol m}^{-2} \text{s}^{-1}$) aggregated from measured EC data.
429 The error bars correspond to ± 1 S.D. of aggregated fluxes for both measured and gap-filled EC
430 values. The horizontal dashed line indicates zero fluxes.

431 At the hourly to diel scale, we found that certain times of day had higher fluxes than
432 others, but that overall, there was little difference in fluxes at midday versus midnight. Measured
433 EC fluxes revealed no statistically significant difference between paired CO_2 fluxes measured
434 during the day (11:00 to 13:00) as compared to night (23:00 to 01:00; $p=0.09$; Fig. 4; Table S6),
435 and no statistically significant difference between paired, measured day and night CH_4 fluxes
436 ($p=0.16$; Fig. 4; Table S6). We did observe significantly higher median CO_2 fluxes measured at
437 dawn (05:00 to 07:00; $1.34 \mu\text{mol m}^{-2} \text{s}^{-1}$) as compared to dusk (17:00 to 19:00; $-0.030 \mu\text{mol m}^{-2}$
438 s^{-1} ; $p<0.001$; Fig 4; Table S6), which may be related to higher median dawn wind speeds
439 ($p<0.001$), though there was no statistical difference between dawn and dusk CH_4 fluxes.



440

441 **Figure 4.** Day (11:00 to 13:00) vs. night (23:00 to 01:00) comparisons of A. carbon dioxide
 442 (CO_2 , $\mu\text{mol m}^{-2} \text{s}^{-1}$) fluxes, B. methane (CH_4 , $\mu\text{mol m}^{-2} \text{s}^{-1}$) fluxes, and C. wind speed (m s^{-1})
 443 measured using the eddy covariance (EC) system deployed at Falling Creek Reservoir. Points
 444 represent measured half-hourly fluxes, while the boxes represent the 25th and 75th percentile,
 445 respectively and the thick line shows the median flux calculated with measured EC data. Dawn
 446 (05:00 to 07:00) vs. dusk (17:00 to 19:00) comparisons of D. CO_2 fluxes, E. CH_4 fluxes, and F.
 447 wind speed. Wilcoxon signed-rank tests were used to determine statistical significance between
 448 paired (day to night; dawn to dusk) fluxes. Statistical significance was defined a priori as $p < 0.05$;
 449 asterisks indicate statistically significant differences. n indicates the number of paired fluxes
 450 (Table S6).

451 At the seasonal scale, both CO_2 and CH_4 fluxes (EC and diffusive measured fluxes) were
 452 greater in magnitude and more variable during the summer than winter, with increasing fluxes
 453 during the late spring and decreasing fluxes during the late fall (Figs. 2, 3). During the summer
 454 months (June – August), FCR was an overall source of CO_2 and CH_4 to the atmosphere for both

455 years (Figs. 2, 3). Specifically, CO₂ and CH₄ fluxes were up to 5× and 15× greater, respectively,
456 during the summer stratified period (May – October) as compared to the winter and early spring
457 (November – April; Fig. 2, 3, S9). During fall turnover, EC measured CO₂ fluxes remained low
458 in both years (2020, 2021), while diffusive fluxes showed an increase in CO₂ fluxes on the day
459 of turnover (Figs. 2, S11). Similarly, CH₄ fluxes were also low during and following turnover for
460 both EC and diffusive fluxes in both years (Figs. 3, S9). From September to April, FCR was a
461 small CO₂ source, but emitted less CO₂ than during the summer. For CH₄, FCR was almost net
462 neutral from late fall to early spring (November to April), in contrast to larger CH₄ emissions
463 during the summer. Following the onset of spring mixing, there was a small, but notable increase
464 in CO₂ emissions in 2021 but little change in CH₄ emissions. In 2022, there were no notable
465 changes in either CO₂ or CH₄ fluxes following ice-off and subsequent spring mixing in 2022
466 (Fig. 5). At the annual scale, there were notably higher CO₂ fluxes in the late-summer and early
467 fall 2021 as compared to the summer and fall 2020, while for CH₄ fluxes, there were notably
468 higher fluxes both in the mid-summer 2021 and in the late-summer and early fall 2021 (Figs. 2,
469 3).

470 3.2 Comparison of EC and diffusive fluxes

471 Overall, both CO₂ and CH₄, diffusive fluxes were within the range of measured EC
472 fluxes, though diffusive CO₂ fluxes were lower than measured EC fluxes when comparing
473 discrete timepoints (Fig. 2, 3; Table S5). Specifically, hourly CO₂ diffusive fluxes calculated
474 from grab surface samples were an order of magnitude lower than measured EC fluxes and
475 ranged from -1.24 to 17.50 μmol m⁻² s⁻¹, with a mean flux of 0.39 ± 1.29 μmol m⁻² s⁻¹ (Figs. 2,
476 S10, S11; Table S5). We note that the magnitude of diffusive fluxes was highly sensitive to the
477 gas transfer coefficient method (k) used in flux calculations, and thus we presented the mean and
478 standard deviation of the seven different k models used, which represent the range of possible
479 diffusive fluxes which could be compared to EC measured fluxes (Eq. 1; Fig. S10). Hourly CH₄
480 diffusive fluxes were more comparable to measured EC fluxes, with a range of -0.003 to 0.096
481 μmol m⁻² s⁻¹ and a mean of 0.006 ± 0.009 μmol m⁻² s⁻¹ (Figs. 3, S10, S11; Table S5).

482 3.3 Environmental predictors of CO₂ and CH₄ fluxes

483 During the study period, FCR experienced typical meteorological and environmental
484 conditions. The meteorology measured at the reservoir dam recorded a mean air temperature of
485 14.1°C (13.8 and 14.4°C in years 1 and 2, respectively), with a minimum and maximum
486 temperature of -11.5 and 35.1°C, respectively across the two years (Table S7). Mean wind speed
487 during the time period was 1.99 m s⁻¹ (2.00 and 1.97 m s⁻¹ for years 1 and 2, respectively), with a
488 maximum wind speed of 11.2 m s⁻¹ and a dominant wind direction of 198° (191° and 199° for
489 years 1 and 2, respectively). Yearly total rainfall ranged from 790 mm (Year 2) to 1438 mm
490 (Year 1). During the winter (January - February), air temperatures in year 1 ranged from -8.0 to
491 19.4°C with a mean of 1.9°C and in year 2 ranged from -11.5 to 21.4°C with a mean of 2.1°C.

492 Water column variables measured at 1.6 m below the surface also exhibited typical
493 annual patterns and were for the most part similar between years. We found water temperatures
494 ranged from 1.23 to 31.4°C, with a mean of 15.2 and 15.9°C for years 1 and 2, respectively (Fig.
495 S6; Table S8). Chl-a values ranged from 0.25 to 121 µg L⁻¹, with a mean of 11.5 µg L⁻¹ and 12.3
496 µg L⁻¹ in years 1 and 2, respectively. fDOM was also nearly identical in years 1 and 2 with a
497 mean of 6.09 and 6.04 RFU, respectively, and a range of 3.01 to 10.4 RFU. For DO sat., the
498 mean was 107 and 97.8% in year 1 and year 2. Finally, inflow was higher in year 1 (0.056 m³ s⁻¹)
499 as compared to year 2 (0.013 m³ s⁻¹) and ranged from 0.005 to 0.27 m³ s⁻¹ (Fig. S7; Table S8).
500 This resulted in a substantial difference in calculated water residence time, with substantially
501 lower mean water residence time in year 1 (148 ± 169 d) as compared to year 2 (347 ± 119 d;
502 Fig. S1).

503 Overall, surface water temperature and thermocline depth were found to be the most
504 important environmental predictors for both CO₂ and CH₄ fluxes over all timescales analyzed
505 (daily, weekly, monthly), followed by fDOM (Table 1). Inflow discharge was only intermittently
506 important for CO₂ and CH₄ fluxes at various timescales while DO sat. and Chl-a were only
507 intermittently important for CO₂ fluxes (Tables 1, S9). Water temperature was positively
508 correlated with both CO₂ and CH₄ fluxes at all timescales, following the pattern of higher GHG
509 fluxes during summer as compared to winter in the time series data (Figs. 2, 3). CO₂ fluxes were
510 negatively associated with thermocline depth while CH₄ fluxes were positively associated with

511 thermocline depth at all timescales (Table 1); i.e., CO₂ fluxes were greater when there were
512 shallower thermocline depths, whereas CH₄ fluxes were greater when there were deeper
513 thermocline depths.

514 In addition to water temperature and thermocline depth, CO₂ fluxes were positively
515 associated with fDOM across all timescales, while CH₄ fluxes were only positively associated
516 with fDOM at the daily and weekly timescales (Table 1). Conversely, inflow was positively
517 associated with CO₂ fluxes at daily and weekly timescales, while inflow was negatively
518 associated with CH₄ fluxes at weekly and monthly timescales. Finally, Chl-a was negatively
519 associated with CO₂ fluxes, but only on the daily timescale and was negatively associated with
520 DO sat. at the weekly timescale. CH₄ fluxes were not associated with either Chl-a or DO sat. at
521 any timescale.

522 CO₂ fluxes were best predicted by ARIMA models at the monthly timescale
523 (RMSE=0.48 μmol m⁻² s⁻¹), with descending RMSE for the weekly (0.63 μmol m⁻² s⁻¹) and then
524 daily (0.97 μmol m⁻² s⁻¹) models (Tables 1; S9). For CH₄ fluxes, the best-fitting ARIMA model
525 was also identified at the monthly timescale (RMSE=0.41 μmol m⁻² s⁻¹), with descending RMSE
526 for the weekly and daily models ranging from 0.64 and 1.02 μmol m⁻² s⁻¹, respectively (Tables 1,
527 S8). Full ARIMA results are reported in Table S9.

528 **Table 1.** Best-fit results from Autoregressive Integrated Moving Average (ARIMA) analysis

GHG	Timescale	Model Order	Surface Temp (°C)	DO Sat. (%)	Chl-a ($\mu\text{g L}^{-1}$)	fDOM (RFU)	Inflow ($\text{m}^3 \text{s}^{-1}$)	Thermo. Depth (m)	RMSE ($\mu\text{mol m}^2 \text{s}^{-1}$)
CO2	Daily	(1,0,0)	0.18	-	-0.17	0.07	0.08	-0.09	0.97
	Weekly	(0,0,0)	0.64	-0.16	-	0.13	0.20	-0.19	0.63
	Monthly	(0,0,0)	0.73	-	-	0.24	-	-0.31	0.48
CH4	Daily	(0,0,0)	0.27	-	-	0.12	-	0.25	1.02
	Weekly	(0,1,1)	0.36	-	-	0.23	-0.36	0.24	0.64
	Monthly	(0,0,1)	0.74	-	-	-	-0.26	0.21	0.41

529

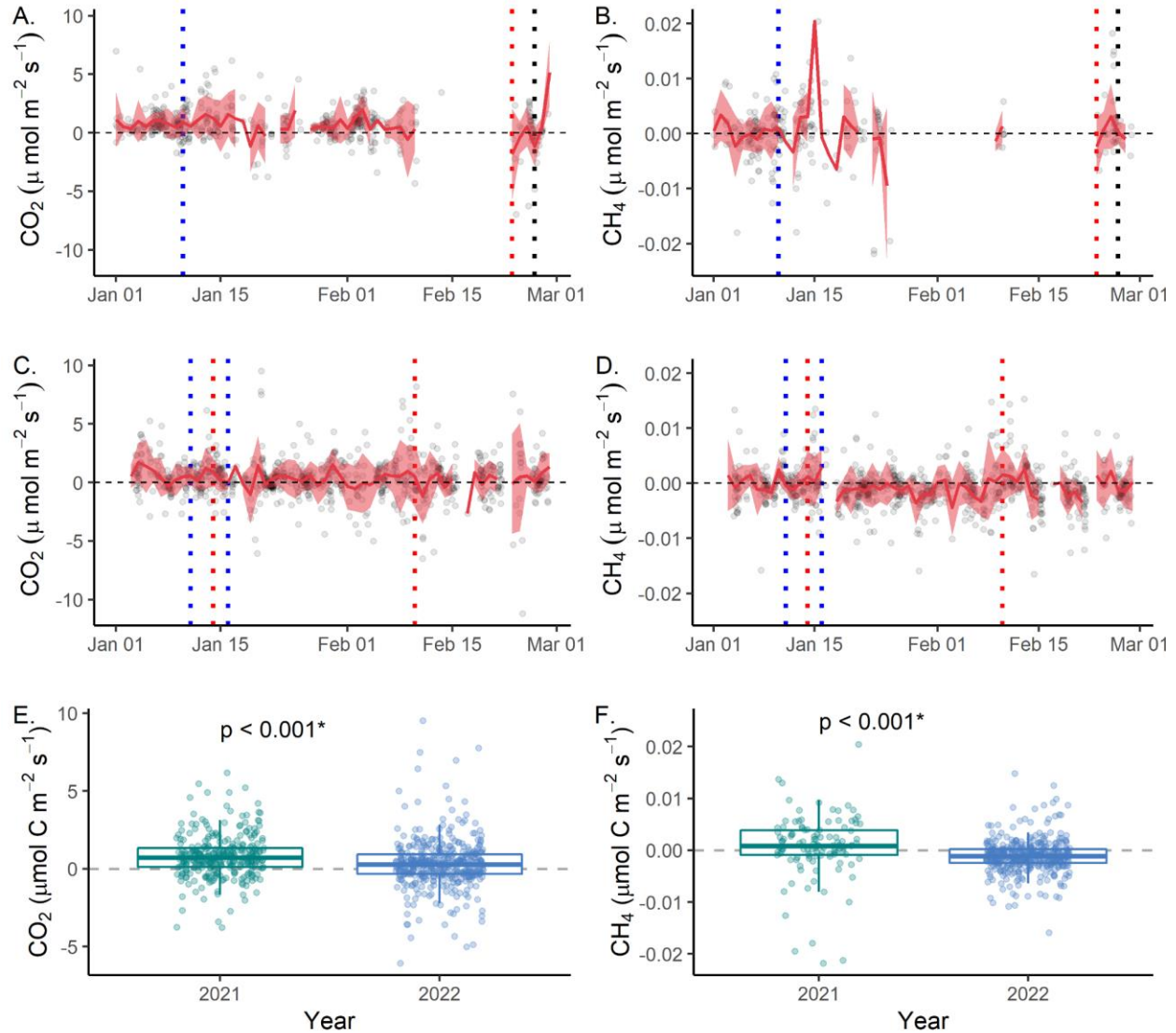
530 *Note:* Table includes only the top selected model (lowest corrected Akaike Information Criterion, AICc). Models are separated by
 531 greenhouse gas (GHG) flux as carbon dioxide (CO₂) and methane (CH₄) fluxes as well as by timescale (daily, weekly, monthly).

532 Environmental predictors included: Surface temperature (Surface Temp, °C), dissolved oxygen saturation (DO Sat, %), Chlorophyll-*a*
 533 (Chl-*a*, $\mu\text{g L}^{-1}$), fluorescent dissolved organic matter (fDOM, RFU), inflow discharge (Inflow, $\text{m}^3 \text{s}^{-1}$), and thermocline depth
 534 (Thermo. Depth, m). Model order is specified as (p,d,q) where p is the order of the AR term, d is the order of the integration term, and
 535 q is the order of the MA term. For brevity, the autoregressive (AR) and moving average (MA) terms have been removed but can be
 536 found in the supplemental information. Results for all models with 2 AICc of the best fitting model, can be found in the supplemental
 537 information (Table S9). Dashed lines indicate environmental parameters that were not identified as statistically significant. The root
 538 mean square error (RMSE) is reported for each model. Standard errors for each parameter value are given in Table S9.

539 3.4 Influence of ice cover on CO₂ and CH₄ fluxes

540 FCR experienced two distinct winter regimes in 2021 vs. 2022. In 2021, ice-on first
541 occurred on 10 January 2021, then came on and off multiple times before final ice-off on 23
542 February 2021. Overall, there were 27 days with some ice and 9 days with some open-water
543 during the 2021 intermittent ice-period. In contrast, in 2022, there was a brief period of ice cover
544 from 11 January to 14 January 2022, followed by continuous ice-on occurring from 16 January
545 2022 to final ice-off on 10 February 2022. While we were unable to collect ice thickness data
546 through both winters due to safety concerns, peak ice thickness in FCR in 2022 was ~9.5 cm
547 whereas peak ice thickness in 2021 was ~2 cm.

548 When comparing measured half-hourly fluxes aggregated across the intermittent ice-on
549 period in winter 2021 and the continuous ice-on period in winter 2022, there were statistically-
550 significantly higher median CO₂ and CH₄ fluxes measured during intermittent ice-on than
551 continuous ice-on (Kruskal-Wallis $p < 0.0001$; Fig. 5; Table S10). During intermittent ice-on in
552 winter 2021, median CO₂ fluxes were 0.71 $\mu\text{mol m}^{-2} \text{s}^{-1}$, 2.5 \times higher than the median of 0.28
553 $\mu\text{mol m}^{-2} \text{s}^{-1}$ during continuous ice-on in 2022. For CH₄, median fluxes were 0.001 $\mu\text{mol m}^{-2} \text{s}^{-1}$
554 and -0.001 $\mu\text{mol m}^{-2} \text{s}^{-1}$, during intermittent ice-on and continuous ice-on, respectively (Table
555 S10). Throughout the winter period, mean daily CO₂ and CH₄ fluxes were much lower and less
556 variable than in the summer, for both years (Fig. 2, 3).



557

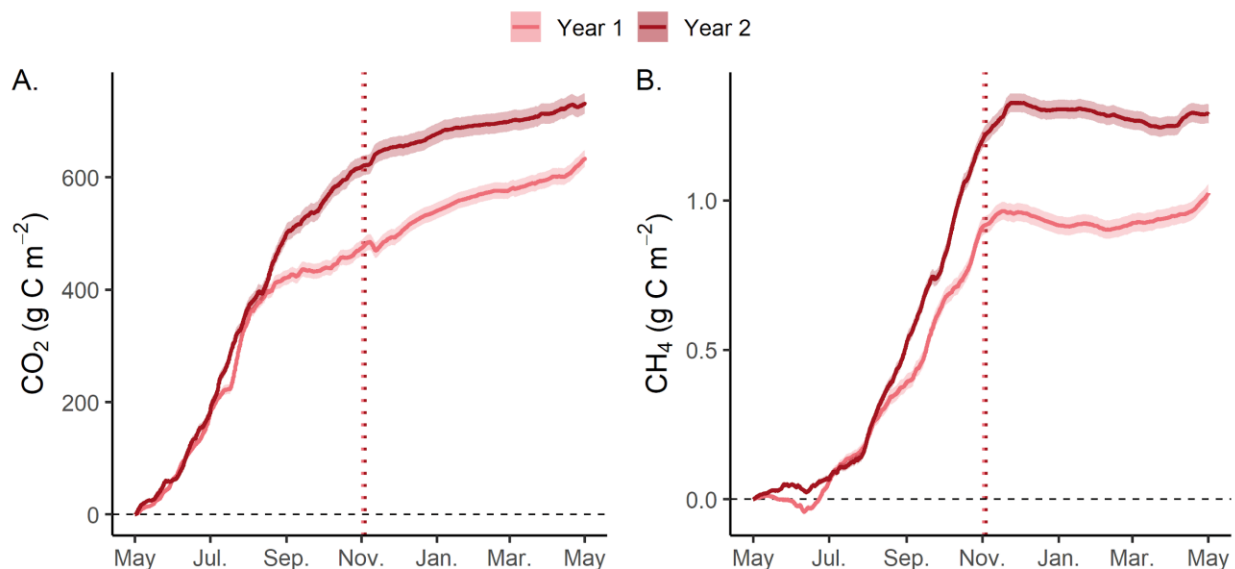
558 **Figure 5.** Mean daily fluxes during the winter of 2021 for A. Carbon dioxide (CO₂, μmol m⁻² s⁻¹)
 559 and B. Methane (CH₄ μmol m⁻² s⁻¹) during intermittent ice-on. Mean daily fluxes during winter
 560 of 2022 for C. CO₂ and D. CH₄ during near-continuous ice-on. Grey dots represent measured
 561 half-hourly fluxes while the solid red line indicates mean daily fluxes. The shaded red area
 562 corresponds to the standard deviation (±1 S.D.) of the daily mean fluxes. The blue vertical
 563 dashed lines correspond to the start of either intermittent or near-continuous ice-on for winter
 564 2021 and 2022, respectively, while the red vertical dashed lines correspond to the start of
 565 complete ice-off. The black dashed line in 2021 corresponds to spring mixing (first day after ice-
 566 off when the temperature at 1 m and 8 m was < 1°C). For 2022, spring mixing was on the same
 567 day as ice-off. Boxplots of measured E. CO₂ and F. CH₄ fluxes during each winter's intermittent
 568 or continuous ice-on, respectively. For each box plot, the median is represented as the bold line
 569 while the 25th and 75th percentiles are represented as the bottom and top of the box, respectively.
 570 The whiskers represent minimum and maximum values (1.5× interquartile range). Points
 571 represent all half hourly fluxes measured during the respective winter intermittent or continuous
 572 ice-on, respectively period. The dashed horizontal line corresponds to zero fluxes. Asterisks

573 indicate statistically significant differences between median half-hourly fluxes measured during
574 intermittent (2021) and continuous (2022) ice-on periods using Mann-Whitney-Wilcoxon tests (α
575 = 0.05).

576 3.5 Net CO₂ and CH₄ balance for a small, eutrophic reservoir

577 Gap-filled CO₂ and CH₄ half-hourly fluxes summed across the entire year indicate that
578 FCR was an overall source of CO₂ and CH₄ to the atmosphere (Fig. 6). According to gap-filled
579 EC fluxes, FCR released 633 and 731 g CO₂-C m⁻² year⁻¹, during the first and second years of the
580 study, respectively. For gap-filled CH₄ fluxes, FCR released 1.02 and 1.29 g CH₄-C m⁻² year⁻¹,
581 respectively. Although substantial gap-filling was needed, the gap-filled and measured data
582 yielded similar estimates when the measured data were scaled by the percentage of missing data
583 from the measured time series (Fig. S12).

584 The annual GHG balances were driven by large fluxes of CO₂ and CH₄ during the
585 summer. Net emissions during the warmest months (June – September; 375 and 496 g CO₂-C m⁻²
586 for year 1 and year 2, respectively) represented up to 68% of the total annual net CO₂ flux as
587 compared to the coldest months (December – March) when only 98 and 57 g CO₂-C m⁻² was
588 emitted (up to 15% of the total annual CO₂). Similarly, for CH₄, up to 66% of the total annual net
589 CH₄ flux was released during the warmest months (June – September; 0.67 and 0.76 g CH₄-C m⁻²
590 ²) and less than 1% during the coldest months (December – March). For the second year of
591 monitoring, annual fluxes were greater for both CO₂ and CH₄, largely due to elevated fluxes in
592 early and late fall (September – November). Cumulatively, the amount of CO₂-C released from
593 FCR was three orders of magnitude greater than the mass of CH₄-C released.



594

595 **Figure 6.** Annual cumulative fluxes using measured and gap-filled eddy covariance (EC) data
 596 for A. carbon dioxide (CO₂, g C m⁻²) and B. methane (CH₄, g C m⁻²) from Falling Creek
 597 Reservoir for Year 1 (May 2020-April 2021; pink) and Year 2 (May 2021-April 2022; dark red).
 598 Shaded areas correspond to the aggregated standard deviation (± 1 S.D.) of measurements. The
 599 horizontal dashed line corresponds to zero and the vertical dotted line indicates reservoir fall
 600 turnover for both years.

601

602 **4 Discussion**

603 This study provides the first annual-scale, multi-year estimates of *both* CH₄ and CO₂
 604 fluxes using an EC system from a small reservoir. While using EC systems in small freshwaters
 605 is inherently challenging and contains several limitations, our work reveals variable patterns in
 606 both CO₂ and CH₄ fluxes over sub-daily to seasonal scales that set the stage for future work. Our
 607 study was limited by low levels of measured data, underscoring the need for more accurately
 608 quantifying the GHG contributions of small reservoirs on multiple timescales. Despite these
 609 challenges, however, our data suggest that FCR was a substantial CO₂ and CH₄ source to the
 610 atmosphere on multiple timescales. Below we discuss some of the challenges of using an EC
 611 system in small freshwaters as well as the patterns and potential drivers of variability in fluxes
 612 (CO₂ and CH₄) over multiple timescales, including during winter ice-cover.

4.1 Variability in sub-daily fluxes, with higher dawn than dusk CO₂ fluxes

A key advantage of an EC system is the ability to capture variability in sub-daily GHG fluxes throughout the year. Despite data gaps and limitations, the fluxes collected by the EC represent a substantial increase in the ability to identify variability in GHG fluxes at multiple timescales. Our work complements previous studies of freshwater systems using EC measurements that observed high sub-daily variability in both summer CO₂ (Liu et al. 2016; Golub et al. 2021; Shao et al. 2015) and CH₄ fluxes (Eugster et al. 2011; Podgrajsek et al. 2014; Taoka et al. 2020; Waldo et al. 2021) and furthers our understanding of the variability of CO₂ and CH₄ fluxes on multiple timescales.

When comparing day (11:00 to 13:00) versus night (23:00 to 01:00) fluxes, we observed no statistically significant differences between CO₂ or CH₄ fluxes using measured EC fluxes aggregated over the two-year monitoring period (Fig. 4; Table S6). When repeating this analysis separately among seasons, we did observe a statistically significant difference between day and night for CH₄ fluxes during the winter, but that was the only season where statistical differences were detected (Table S11). Similarly, studies in a small Finnish lake also found no evidence for diel differences in CO₂ fluxes (Erkkiliä et al. 2018; Mammarella et al. 2015), while Waldo et al. (2021) found diel differences in CH₄ fluxes on only 18.5% of days out of a 2-year study period. Other studies, however, have observed more consistent diel patterns in GHG fluxes. For example, some studies have shown higher CH₄ fluxes during the night in lakes and reservoirs (Eugster et al. 2011; Podgrasjek et al. 2014; Waldo et al. 2021) and higher CO₂ fluxes at night in streams (Attermeyer et al. 2021; Gómez-Gener et al. 2021). On the other hand, some studies observed higher CH₄ fluxes during the day as compared to night (Erkkiliä et al. 2018; Jammet et al. 2017; Podgrasjek et al. 2016; Sieczko, et al. 2020). Our results are contrary to our predictions, in which we expected statistically higher CO₂ fluxes during the day due to significantly higher wind speeds. We hypothesize that higher concentrations of dissolved CO₂ in the surface waters at night, due to decreased primary productivity and elevated microbial respiration or convective mixing of deeper waters with higher dissolved GHG concentrations (Liu et al. 2016; Fig. S13), were not efficiently transferred to the atmosphere at the low observed nightly wind speeds, resulting in similar flux magnitudes during both day and night. Clearly, there is a range of responses to diel variation among lake and reservoir CO₂ and CH₄ fluxes, and more work is

643 needed to identify when, where, and why lakes and reservoirs may emit differential GHGs
644 during day vs. night.

645 While we did not observe statistically significant differences between GHG fluxes
646 measured during the day as compared to night, we did observe statistically significantly higher
647 CO₂ fluxes at dawn (05:00 to 07:00) as compared to dusk (17:00 to 19:00), but no difference in
648 dawn vs. dusk CH₄ fluxes over the full study period (Fig. 4). Similarly, studies conducted in
649 other lakes also found CO₂ flux minima during the late afternoon (~18:00) and CO₂ flux maxima
650 during the early morning (~06:00; Liu et al. 2016; Shao et al. 2015), supporting our observations
651 of higher dawn CO₂ fluxes. Liu et al. (2016) hypothesized the lower CO₂ fluxes observed during
652 the day (~18:00) were likely a result of elevated primary productivity during the afternoon,
653 primarily in the summer months, but could have also been due to convective mixing in the water
654 column at night.

655 Altogether, our results provide additional evidence that the time of sample collection has
656 important implications for upscaling freshwater GHG fluxes to longer timescales (Attermeyer et
657 al. 2021; Gómez-Gener et al. 2021). A previous study conducted in FCR which estimated CO₂
658 and CH₄ diffusive fluxes using discrete GHG measurements collected at ~noon concluded FCR
659 was often a small CO₂ sink during the summer stratified period in 2015-2016 (McClure et al.
660 2018), whereas our diel EC data indicate that FCR was an overall CO₂ source throughout the
661 summer in both 2020 and 2021. While the flux magnitudes measured by McClure et al. (2018)
662 were similar to the present study, the overall conclusions were different due to the temporal
663 resolution of sample collection.

664 4.2 Important role of water temperature and thermocline depth in constraining daily,
665 weekly, and monthly CO₂ and CH₄ fluxes

666 Following our analysis of CO₂ and CH₄ fluxes over daily to seasonal timescales, we then
667 used time-series analysis to test the potential effects of various limnological variables on GHG
668 fluxes. Specifically, ARIMA results show that surface water temperature was positively
669 correlated with both CO₂ and CH₄ fluxes at the daily, weekly, and monthly timescales (Table 1).
670 These results were supported by higher fluxes of both CO₂ and CH₄ observed during the warmer
671 summer months when aggregated to daily, weekly, and monthly timescales (Fig. 2, 3, S8).

672 Strong positive correlations between GHG fluxes (both CO₂ and CH₄) and water temperature
673 have been observed in several freshwater ecosystems, especially on longer timescales, with clear
674 differences between summer and winter fluxes (monthly to seasonally; Eugster et al. 2011; Reed
675 et al. 2018; Taoka et al. 2020). Higher GHG fluxes were expected during the summer as
676 compared to winter, due to elevated rates of biological respiration stimulated by higher
677 temperatures in both the surface and deep waters (Fig. S13). Generally, water column dissolved
678 GHG concentrations increased throughout the summer period (Fig. S13). In the surface waters,
679 dissolved CH₄ concentrations generally peaked in July, while dissolved CO₂ concentrations
680 increased throughout the summer and peaked around fall turnover.

681 In addition to temperature, thermocline depth was also identified as an important
682 environmental parameter controlling both CO₂ and CH₄ fluxes. For CO₂ fluxes, thermocline
683 depth was negatively associated with fluxes at all timescales, indicating higher CO₂ fluxes when
684 the thermocline was shallower. Generally, thermocline depth was shallower in the late summer
685 (Fig. S7) when CO₂ fluxes were observed to be greatest and most variable in FCR. This pattern
686 may be indirectly related to water temperature, as shallower thermocline depths were weakly,
687 negatively associated with warmer water temperatures, and there was a strong positive
688 relationship between CO₂ fluxes and water temperature, as discussed above.

689 Conversely, thermocline depth was positively correlated with CH₄ fluxes at all timescales
690 (daily, weekly, monthly), indicating higher CH₄ fluxes when the thermocline depth was deeper,
691 which was generally observed during the late summer and early fall as mixing increased (Fig.
692 S7). Previous studies have suggested water column mixing is an important control on CH₄
693 fluxes, leading to higher fluxes during convective and wind-driven mixing when high dissolved
694 concentrations of CH₄ accumulated in the deeper waters are mixed to the surface, which would
695 be more common when the thermocline depth is deeper (Sieczko et al. 2021). We did observe
696 elevated dissolved CH₄ concentrations in the metalimnion (3.8 - 5 m), particularly in the late
697 summer and early fall when the thermocline started to deepen (Fig. S7, S13), which was likely
698 mixed into the surface waters and contributed to reservoir CH₄ fluxes, as observed previously in
699 FCR by McClure et al. (2018). However, we do not know the extent of methanotrophy in
700 converting dissolved CH₄ to CO₂ prior to emissions. While we also observed elevated dissolved
701 CO₂ concentrations at similar depths during the late summer and early fall, we might expect

702 elevated primary production observed at this same time (Fig. S6) reduced overall fluxes of CO₂
703 from the reservoir. Additional research is needed to specifically link water column dissolved
704 GHG concentrations and water column processes with atmospheric emissions.

705 Following temperature and thermocline depth, fDOM was identified as a key positive
706 environmental predictor for CO₂ fluxes at all timescales (daily, weekly, monthly; Table 1). A
707 similar positive relationship between terrestrially-derived DOM and dissolved CO₂ was
708 identified in 48 Canadian streams (D'Amario and Xenopoulos, 2015). As fDOM sensors are
709 thought to mainly capture allochthonous DOM (Howard et al. 2021; Watras et al. 2015), this
710 finding suggests that allochthonous DOM from the reservoir's primary inflow stream or diffuse
711 overland flow may result in elevated CO₂ emissions from freshwater ecosystems as
712 allochthonous DOM is converted to CO₂ during respiration. This follows previous research
713 which has identified allochthonous carbon inputs and associated DOC concentrations as
714 important predictors of CO₂ fluxes in lakes and reservoirs (Barros et al. 2011; Sobek et al. 2005).
715 Unlike for CO₂, fDOM was only identified as an important environmental predictor for CH₄
716 fluxes at shorter timescales (daily, weekly). In an analysis of >300 lakes, Sanches et al. (2019)
717 found a strong positive relationship between dissolved organic C and diffusive CH₄ fluxes,
718 suggesting dissolved organic C availability for methanogenesis may play an important role in
719 constraining CH₄ fluxes across multiple lakes and timescales. The strong positive correlation
720 between CH₄ fluxes and fDOM observed here further indicates that dissolved organic C, as a
721 proxy from fDOM (Howard et al. 2021), may also be important at the local scale on short-
722 timescales.

723 In addition to these overarching patterns, several environmental parameters were
724 intermittently important for various timescales for either CO₂ or CH₄ fluxes. CO₂ fluxes were
725 positively correlated with inflow at shorter timescales (daily, weekly) while CH₄ fluxes were
726 negatively correlated with inflow but only at longer timescales (weekly, monthly; Table 1).
727 Following the positive relationship between CO₂ fluxes and fDOM, we hypothesize the positive
728 relationship with inflow reflects the importance of allochthonous DOM delivery to FCR via the
729 primary inflow and diffuse overland flow, which suggests a potentially labile source of
730 allochthonous DOM to the reservoir via the primary inflow. Pearson correlation analysis,
731 suggests fDOM and inflow were weakly correlated at these timescales (daily, weekly; $\rho = 0.13$,

732 0.11, respectively), but was weakly negatively correlated at longer timescales (monthly, $\rho = -$
733 0.03; Table S4). Previous research examining CH₄ fluxes from FCR have found similar negative
734 relationships between inflow and CH₄ fluxes, especially via ebullition in the upstream, littoral
735 portion of the reservoir (McClure et al. 2020). Results from this study suggest inflow is similarly
736 correlated with CH₄ fluxes at the deepest point of the reservoir, primarily on longer timescales
737 (weekly, monthly). Finally, Chl-a was negatively associated with CO₂ fluxes at the daily
738 timescale while DO sat. was negatively associated with CO₂ fluxes at the weekly timescale
739 (Table 1). Both of these relationships suggest a coupling between high primary production, as
740 indicated by high Chl-a and high DO Sat., and low CO₂ fluxes on shorter timescales (daily,
741 weekly). Previous studies have identified a weak negative relationship between primary
742 production and CO₂ fluxes on the sub-daily timescale in other eutrophic, freshwater lakes and
743 reservoirs (Liu et al. 2016; Shao et al. 2015).

744 4.3 Role of fall turnover and ice cover in affecting GHG dynamics

745 Contrary to previous studies conducted in both FCR and other thermally-stratified
746 waterbodies (e.g., Erkkilä et al. 2018; McClure et al. 2018; 2020), we observed low CO₂ and
747 CH₄ fluxes during the days surrounding fall turnover for both years (1 November 2020; 3
748 November 2021), when EC data indicate that FCR was a small to negligible CO₂ and CH₄ source
749 (Fig. 2, 3, S9). Discrete diffusive fluxes measured on the day of fall turnover suggest FCR was a
750 4x and 14x larger CO₂ source than fluxes measured with the EC, in years 1 and 2 respectively
751 (Figs. 2, S9). Similar to CO₂, we found the magnitude of CH₄ fluxes decreased following fall
752 turnover but remained a small source (Fig. 3, S9). McClure et al. (2018) observed episodic
753 release of CH₄ from FCR during the weeks prior to fall turnover as high concentrations of
754 dissolved CH₄ that had accumulated in the middle of the water column, due to the formation of a
755 metalimnetic oxygen minimum, were emitted during wind-mixing. In the weeks prior to fall
756 turnover, we did observe elevated CH₄ emissions in both years (Figs. 3, S9), supporting this
757 observed mechanism (McClure et al. 2018; Fig. S13), and decreasing the importance of fall
758 turnover as a single pulse of emissions. For CO₂, similar increases in dissolved CO₂
759 concentrations were observed in the metalimnion during the same time period, but as suggested
760 above, the release of this CO₂ to the atmosphere was likely mitigated by primary production in
761 the surface waters.

762 Importantly, this study provides some of the first near-continuous flux measurements of
763 *both* CO₂ and CH₄ during winter, including during intermittent and continuous ice-on conditions
764 (Fig. 5). Overall, the annual GHG balance was driven by large fluxes of CO₂ and CH₄ during the
765 summer, as CO₂ and CH₄ fluxes were 3× and 23× greater, respectively, during the summer
766 stratified period (April – October) as compared to the winter and early spring (November –
767 March; Fig. 6). However, we do note that we observed significantly higher CO₂ and CH₄ fluxes
768 during intermittent ice-on when there is likely more air-water gas exchange as compared to
769 continuous ice-on ($p < 0.001$; Fig. 5; Table S10), which would physically limit air-water gas
770 exchange, thereby demonstrating the importance of annually-variable, winter ice dynamics to
771 seasonal GHG fluxes. Of the studies that report GHG fluxes during continuous ice-on, all report
772 low fluxes with low variability (A.K. Baldocchi et al. 2020; Jammet et al. 2015, 2017; Reed et al.
773 2018), similar to the winter with continuous ice-on at FCR. Interestingly, these studies also noted
774 high fluxes immediately following ice-off for both CO₂ and CH₄ due to accumulation of
775 dissolved CO₂ and CH₄ under the ice from aerobic and anaerobic microbial respiration
776 (Anderson et al. 1999; A.K. Baldocchi et al. 2020; Gorsky et al. 2021; Jammet et al. 2015, 2017;
777 Podgrajsek et al. 2015; Takoa et al. 2020), which was not observed at FCR. Unlike these
778 previous studies, which were largely conducted in northern lakes which are frozen for months at
779 a time, FCR is a more temperate system which only periodically freezes for a few days to weeks
780 at time (Carey and Breef-Pilz, 2022). We hypothesize that the brief continuous ice-cover
781 observed at FCR during winter 2022 (25 days) was not long enough to promote extensive
782 accumulation of dissolved GHGs under ice, as observed by the other studies. Further work on the
783 effect of ice cover on GHG fluxes is needed, but our comparison of intermittent ice-on vs.
784 continuous ice-on suggests that the increasing intermittent ice-cover being experienced in many
785 lakes worldwide (Imrit and Sharma, 2021; Sharma et al. 2021; Woolway et al. 2020) will likely
786 increase winter GHG fluxes. These increases may be due to both greater continuous exchange of
787 GHGs across the air-water interface and increased rates of microbial respiration under higher
788 winter temperatures.

789 4.4 Much higher annual CO₂ emissions from FCR than other studied reservoirs

790 When scaling fluxes to the full year, FCR was a much smaller annual CH₄ source (1.02-
791 1.29 g m⁻² yr⁻¹), yet a larger CO₂ source (633-731 g m⁻² yr⁻¹; Figs. 5, S12), than other reservoirs

792 reported in the literature to date (A.K. Baldocchi et al. 2020; Deemer et al. 2016; Golub et al.
793 2021). While the total magnitude of CO₂ emissions from FCR was greater than most studies,
794 Golub et al. (2021) similarly found that data from 12 lakes and reservoirs over multiple years
795 emitted substantial amounts of CO₂ in their synthesis of EC measured CO₂ fluxes in freshwaters
796 (13.6 - 224 g C m⁻² yr⁻¹), except for one reservoir during one year which had a CO₂ flux of -53.6
797 g C m⁻² yr⁻¹. As compared to other reservoirs with GHG flux data, FCR is old (>100 years old)
798 which may lead to lower GHG emissions, particularly for CH₄ fluxes, likely as a result of
799 reduced supply of organic matter substrate in the sediments as the reservoir ages (Barros et al.
800 2011; McClure et al. 2020; Prairie et al. 2018).

801 Despite its age, however, FCR was a much larger CO₂ source as compared to other lakes
802 and reservoirs. The CO₂ emissions were consistently high among years, suggesting that FCR
803 may be a greater source of CO₂ than most terrestrial environments (-750 to 250 g C m⁻² yr⁻¹ for
804 multi-year, undisturbed terrestrial sites; D.D. Baldocchi et al. 2020). Comparisons between years
805 suggest that slightly higher annual fluxes of CO₂ and CH₄ in the early to late fall (September -
806 November) of the first monitoring year as compared to the second year may be related to slightly
807 higher mean air temperatures or lower inflow levels (and corresponding longer hydraulic
808 residence times), though this remains unknown. We note that these cumulative fluxes are likely
809 conservative, as there were substantial gaps in measured EC fluxes during year 1, particularly in
810 August 2020, likely resulting in underestimated measured fluxes during this time of year when
811 fluxes are usually highest (Fig. 6, S12). Multiple meteorological, biological, and environmental
812 processes likely contributed to the higher observed annual CO₂ fluxes as compared to other lakes
813 and reservoirs. Additional studies comparing GHG fluxes from multiple reservoirs
814 simultaneously are needed to identify these variables.

815 4.5 Challenges of using EC systems in small, freshwater lakes and reservoirs

816 While the study described here greatly expands the temporal frequency of measured CO₂
817 and CH₄ fluxes from a small reservoir, several caveats must be taken into consideration. EC
818 systems are notoriously difficult to use in freshwater ecosystems due to footprint considerations
819 (Vesala et al. 2006), frequent occurrences of low u* values, particularly at night (Vesala et al.
820 2006; Scholz et al. 2021), as well as general considerations resulting in high percentages of data

821 removed due to these and other issues (yielding data coverage of 10 – 40%; e.g., A.K. Baldocchi
822 et al. 2020; Erkkiliä et al. 2018; Huotari et al. 2011; Ouyang et al. 2017; Shao et al. 2015; Waldo
823 et al. 2021; Table S1). While low data coverage was common in the current study, data gaps
824 were relatively consistent across timescales (daily to seasonally) to ensure unbiased data.
825 Furthermore, compared to the temporal frequency of many grab sample methods (i.e., samples
826 measured weekly, biweekly, or monthly), the data coverage of the EC system is still a substantial
827 improvement and more accurately captures fluxes across multiple timescales challenging to
828 sample, such as at night, during winter ice-cover, and during episodic events, such as fall
829 turnover. Importantly, we note that standard gap-filling routines for EC flux data collected from
830 freshwater ecosystems (i.e., lakes and reservoirs) do not currently exist. We applied gap-filling
831 routines originally developed for terrestrial ecosystems (Wutzler et al. 2018) to FCR to better
832 estimate annual scale fluxes, which is still a substantial improvement over traditional grab
833 sampling methods.

834 While strict filtering processes were enacted to limit non-local fluxes (i.e., filtering fluxes
835 when the along-wind distance providing 90% of the cumulative contribution was outside the
836 reservoir), we are unable to completely rule out potential non-local processes (e.g., land-lake
837 interactions) which occur outside the footprint and are entrained or advected into the EC
838 footprint area (Esters et al. 2020; Vesala et al. 2006, 2011; Fig. S2). These processes may be
839 particularly important in small freshwaters located in mountainous regions (Scholz et al. 2021).
840 For example, Scholz et al. (2021) found reduced nighttime CO₂ emissions due to low wind
841 speeds and CO₂ sinking from the land to the lake surface at night in a mountainous Swiss lake.
842 While the topography at FCR is not as extreme, similar processes may be occurring at FCR,
843 though at a smaller scale. In addition, based on studies conducted in similar terrestrial
844 ecosystems, we might expect negative CO₂ fluxes in the summer followed by substantial CO₂
845 emissions in the fall and winter; however, these patterns were not observed in FCR, suggesting
846 the majority of fluxes measured in this study likely originated in the reservoir. When considered
847 and interpreted cautiously, the data collected by the EC system provides a far more
848 comprehensive time series than what is possible from discrete measurements (Anderson et al.
849 1999; Eugster 2003; Houtari et al. 2011; Jonsson et al. 2008; Scholz et al. 2021), which is critical
850 for increasing our understanding of GHG fluxes from small reservoirs on multiple temporal
851 scales.

852 Finally, comparisons with diffusive grab samples suggest fluxes measured with the EC
853 system were consistently higher than those estimated with diffusive grab samples, especially for
854 CO₂ (Fig 2, S11), which is consistent with previous studies (Scholz et al. 2021, and references
855 therein). Conversely, CH₄ fluxes calculated using the discrete diffusive methods were more
856 comparable to those measured by the EC system (Fig. 3, S11). Discrepancies between EC
857 measured fluxes and diffusive grab samples may be a result of the different spatial resolution of
858 the two methods, where the EC system is measuring fluxes both at the deepest point of the
859 reservoir in addition to upstream and littoral portions of the reservoir while diffusive grab
860 samples were only collected at the deepest point of the reservoir (Fig. 1; Scholz et al. 2021).
861 Indeed, several studies have observed higher CO₂ and CH₄ fluxes in the littoral zone, closer to
862 the shore, which would have been encompassed in the measured EC fluxes but not the diffusive
863 grab samples (Erkkiliä et al. 2018; Scholz et al. 2021; Taoka et al. 2020). A comparison of CH₄
864 fluxes on an inflow to dam transect at FCR observed substantially higher fluxes in the littoral
865 zone, supporting this pattern (McClure et al. 2020).

866

867 **5 Conclusions**

868 Overall, we observed FCR to be a source of CO₂ and CH₄ to the atmosphere on annual
869 timescales. Given the limitations of gap-filling, our calculated annual fluxes (~633-731 g CO₂-C
870 m⁻² yr⁻¹; ~1.02-1.29 g CH₄-C m⁻² yr⁻¹) are only estimates, however, we note their remarkable
871 consistency between years. Importantly, by measuring fluxes near-continuously for a full year,
872 we found winter fluxes (December-March) of both CO₂ and CH₄ to be comparatively smaller
873 (15-25% and <1% of total annual fluxes, respectively) than the summer stratified period (June -
874 September) yet still important for annual GHG fluxes. In addition, measuring GHG fluxes during
875 two winters with contrasting ice-cover, showed significantly higher CO₂ and CH₄ fluxes during
876 intermittent as compared to continuous ice-on. Finally, we identified surface water temperature,
877 thermocline depth, and several other environmental variables (fDOM, inflow) as important
878 drivers of both CO₂ and CH₄ fluxes on multiple timescales. Altogether, our results suggest that
879 CO₂ and CH₄ are highly dynamic on multiple temporal scales and highlight the role of small
880 reservoirs as important GHG sources in global budgets. Ultimately, efforts to scale up small
881 reservoir CO₂ and CH₄ emissions will need to consider how the environmental processes that

882 drive C dynamics in small reservoirs may differ from larger waterbodies, which in turn could
883 alter reservoir fluxes. Given the ubiquity of small (<1 km²) reservoirs in the landscape,
884 quantifying their contributions to the global C cycle is paramount, especially given that our study
885 suggests that they may emit more CO₂ and CH₄ than would be expected from their surface area.

886

887 **Acknowledgments**

888 This project originated in February 2020 and was made possible through creative teamwork
889 spanning international borders amidst a global pandemic. We thank Bobbie Niederlehner,
890 Bethany Bookout, Heather Wander, Abigail Lewis, Whitney Woelmer, Dexter Howard, Nicholas
891 Hammond, Arpita Das, Ryan McClure, Mary Lofton, and Calvin Thomas for their assistance
892 with field collection and laboratory analysis. Zoran Nestic and Vahid Daneshmand provided
893 critical troubleshooting assistance and technical support. Additionally, we thank the Western
894 Virginia Water Authority (WVWA), especially Jamie Morris, for long-term access to field sites
895 and logistical support. We gratefully acknowledge funding from U.S. National Science
896 Foundation grants CNS-1737424, DEB-1753639, DEB-1926050, DBI-1933102, and DBI-
897 1933016; and Fralin Life Sciences Institute at Virginia Tech. We also acknowledge Discovery
898 Grant support to Johnson provided by the Natural Sciences and Engineering Research Council of
899 Canada (NSERC), RGPIN-2020-06252. The authors report no conflicts of interest.

900

901 **Open Research**

902 The eddy covariance dataset and associated QA/QC code for this study can be found in the
903 Environmental Data Initiative (EDI) repository via
904 <https://doi.org/10.6073/pasta/a1324bcf3e1415268996ba867c636489> and [https://portal-](https://portal-s.edirepository.org/nis/mapbrowse?packageid=edi.920.2)
905 [s.edirepository.org/nis/mapbrowse?packageid=edi.920.2](https://portal-s.edirepository.org/nis/mapbrowse?packageid=edi.920.2) (Carey et al. 2022a). Additionally, code
906 used for the timeseries and ARIMA analyses are archived at <https://10.5281/zenodo.742001>
907 (Zenodo; Hounshell et al. 2022). Additional datasets including the meteorological data set
908 (<https://portal-s.edirepository.org/nis/mapbrowse?packageid=edi.143.17>, Carey et al. 2022c),
909 limnological dataset (<https://doi.org/10.6073/pasta/81c6c76f4fe22434a20aa8c00f2d4ad1> and

910 <https://portal-s.edirepository.org/nis/mapbrowse?packageid=edi.518.11>, Carey et al. 2022d),
911 inflow discharge (<https://doi.org/10.6073/pasta/c65755d4c0102dde6e3140c1c91b77d6> and
912 <https://portal-s.edirepository.org/nis/mapbrowse?packageid=edi.923.1>, Carey et al. 2022e), ice-
913 cover (<https://portal.edirepository.org/nis/mapbrowse?packageid=edi.456.4>, Carey and Breef-
914 Pilz, 2022), and dissolved discrete grab greenhouse gas concentrations
915 (<https://doi.org/10.6073/pasta/2fb836492aace4c13b7962f2718be8e5> and [https://portal-
916 s.edirepository.org/nis/mapbrowse?scope=edi&identifier=928&revision=3](https://portal-s.edirepository.org/nis/mapbrowse?scope=edi&identifier=928&revision=3), Carey et al. 2022b)
917 are also archived in the EDI. All data (2020-2022) are available for review in the EDI staging
918 environment and will be published following manuscript acceptance. All data through 2021 have
919 been published to EDI and are available under the Creative Commons License - Attribution.

920 **References**

- 921 Anderson, D.E., Striegl, R.G., Stannard, D.I., Michmerhuizen, C.M., McConnaughey, T.A., &
922 LaBaugh, J.W. (1999). Estimating lake-atmosphere CO₂ exchange. *Limnology and*
923 *Oceanography*, 44(4), 988–1001. <https://doi.org/10.4319/lo.1999.44.4.0988>
- 924 Attermeyer, K., Casas-Ruiz, J.P., Fuss, T., Pastor, A., Cauvy-Fraunié, S., Sheath, D., et. al.
925 (2021). Carbon dioxide fluxes increase from day to night across European streams.
926 *Communications Earth & Environment*, 2(1), 118. [https://doi.org/10.1038/s43247-021-](https://doi.org/10.1038/s43247-021-00192-w)
927 [00192-w](https://doi.org/10.1038/s43247-021-00192-w)
- 928 Baldocchi, A.K., Reed, D.E., Loken, L.C., Stanley, E.H., Huerd, H., & Desai, A.R. (2020).
929 Comparing spatial and temporal variation in lake-atmosphere carbon dioxide fluxes using
930 multiple methods. *Journal of Geophysical Research: Biogeosciences*, 125(12).
931 <https://doi.org/10.1029/2019JG005623>
- 932 Baldocchi, D.D. (2020). How eddy covariance flux measurements have contributed to our
933 understanding of Global Change Biology. *Global Change Biology*, 26(1), 242–260.
934 <https://doi.org/10.1111/gcb.14807>
- 935 Barros, N., Cole, J.J., Tranvik, L.J., Prairie, Y.T., Bastviken, D., Huszar, V.L.M., del Giorgio, P.,
936 & Roland, F. (2011). Carbon emission from hydroelectric reservoirs linked to reservoir
937 age and latitude. *Nature Geoscience*, 4(9), 593–596. <https://doi.org/10.1038/ngeo1211>
- 938 Bartosiewicz, M., Przytulska, A., Lapierre, J., Laurion, I., Lehmann, M.F., & Maranger, R.
939 (2019). Hot tops, cold bottoms: Synergistic climate warming and shielding effects
940 increase carbon burial in lakes. *Limnology and Oceanography Letters*, 4(5), 132–144.
941 <https://doi.org/10.1002/lol2.10117>
- 942 Bastviken, D., Sundgren, I., Natchimuthu, S., Reyier, H., & Gålfalk, M. (2015). Technical Note:
943 Cost-efficient approaches to measure carbon dioxide (CO₂) fluxes and concentrations in
944 terrestrial and aquatic environments using mini loggers. *Biogeosciences*, 12(12), 3849–
945 3859. <https://doi.org/10.5194/bg-12-3849-2015>

946 Bastviken, D., Tranvik, L.J., Downing, J.A., Crill, P.M., & Enrich-Prast, A. (2011). Freshwater
947 Methane Emissions Offset the Continental Carbon Sink. *Science*, 331(6013), 50–50.
948 <https://doi.org/10.1126/science.1196808>

949 Beaulieu, J.J., DelSontro, T., & Downing, J.A. (2019). Eutrophication will increase methane
950 emissions from lakes and impoundments during the 21st century. *Nature*
951 *Communications*, 10(1), 1375. <https://doi.org/10.1038/s41467-019-09100-5>

952 Burba, G., & Anderson, D. (2010). A brief practical guide to eddy covariance flux
953 measurements: principles and workflow examples for scientific and industrial
954 applications. Li-Cor Biosciences. Chicago.
955 https://www.licor.com/env/pdf/eddy_covariance/Brief_Intro_Eddy_Covariance.pdf

956 Burba, G., Schmidt, A., Scott R.L., Nakai, T., Kathilankal, J., Fratini, G., et al. (2012).
957 Calculating CO₂ and H₂O eddy covariance fluxes from an enclosed gas analyzer using an
958 instantaneous mixing ratio. *Global Change Biology*, 18(1), 385-399.
959 <https://doi.org/10.1111/j.1365-2486.2011.02536.x>

960 Burnham, K.P., & Anderson, D.R. (2002). *Model selection and multimodel inference: a practical*
961 *information-theoretic approach*. New York, NY: Springer.

962 Butman, D., Stackpoole, S., Stets, E., McDonald, C.P., Clow, D.W., & Striegl, R.G. (2016).
963 Aquatic carbon cycling in the conterminous United States and implications for terrestrial
964 carbon accounting. *Proceedings of the National Academy of Sciences*, 113(1), 58–63.
965 <https://doi.org/10.1073/pnas.1512651112>

966 Carey, C.C. & Breef-Pliz, A. (2022). Ice cover data for Falling Creek Reservoir, Vinton,
967 Virginia, USA for 2013-2022. (Version 4). [Dataset]. Environmental Data Initiative
968 (EDI). <https://portal.edirepository.org/nis/mapbrowse?packageid=edi.456.4>

969 Carey, C.C., Breef-Pilz, A. & Bookout, B.J. (2022c). Time series of high-frequency
970 meteorological data at Falling Creek Reservoir, Virginia, USA 2015-2021 (Version 14).
971 [Dataset]. Environmental Data Initiative (EDI). [https://portal-](https://portal-s.edirepository.org/nis/mapbrowse?scope=edi&identifier=143&revision=14)
972 [s.edirepository.org/nis/mapbrowse?scope=edi&identifier=143&revision=14](https://portal-s.edirepository.org/nis/mapbrowse?scope=edi&identifier=143&revision=14)

973 Carey, C.C., Breef-Pilz, A., Hounshell, A.G., Lofton, M.E., McClure, R.P., Gerling, A.B., &
974 Woelmer, W.M. (2022e). Discharge time series for the primary inflow tributary entering
975 Falling Creek Reservoir, Vinton, Virginia, USA 2013-2021. (Version 8). [Dataset].
976 Environmental Data Initiative (EDI).
977 <https://doi.org/10.6073/pasta/c65755d4c0102dde6e3140c1c91b77d6>

978 Carey, C.C., Breef-Pilz, A., Woelmer, W.M., & Bookout, B.J. (2022d). Time series of high-
979 frequency sensor data measuring water temperature, dissolved oxygen, pressure,
980 conductivity, specific conductance, total dissolved solids, chlorophyll a, phycocyanin,
981 and fluorescent dissolved organic matter at discrete depths in Falling Creek Reservoir,
982 Virginia, USA in 2018-2021. (Version 6). [Dataset]. Environmental Data Initiative (EDI).
983 <https://doi.org/10.6073/pasta/81c6c76f4fe22434a20aa8c00f2d4ad1>

984 Carey, C.C., Hounshell, A.G., D'Acunha, B.M., Breef-Pilz, A., Thomas, R.Q., & Johnson, M.S.
985 (2022a). Time series of carbon dioxide and methane fluxes measured with eddy
986 covariance for Falling Creek Reservoir in southwestern Virginia, USA during 2020-2022.
987 (Version 1). [Dataset]. Environmental Data Initiative (EDI).
988 <https://doi.org/10.6073/pasta/a1324bcf3e1415268996ba867c636489>

989 Carey, C.C., Hounshell, A.G., McClure, R.P., Gerling, A.B., Lewis, A.S.L., & Niederlehner,
990 B.R. (2022b). Time series of dissolved methane and carbon dioxide concentrations for
991 Falling Creek Reservoir and Beaverdam Reservoir in southwestern Virginia, USA during
992 2015-2021. (Version 6). [Dataset]. Environmental Data Initiative (EDI).
993 <https://doi.org/10.6073/pasta/2fb836492aace4c13b7962f2718be8e5>

994 Cole, J.J., & Caraco, N.F. (1998). Atmospheric exchange of carbon dioxide in a low-wind
995 oligotrophic lake measured by the addition of SF₆. *Limnology and Oceanography*, 43(4),
996 647–656. <https://doi.org/10.4319/lo.1998.43.4.0647>

997 Cole, J.J., Prairie, Y.T., Caraco, N.F., McDowell, W.H., Tranvik, L.J., Striegl, R.G., et. al.
998 (2007). Plumbing the Global Carbon Cycle: Integrating Inland Waters into the Terrestrial
999 Carbon Budget. *Ecosystems*, 10(1), 172–185. <https://doi.org/10.1007/s10021-006-9013-8>

1000 Crusius, J., & Wanninkhof, R. (2003). Gas transfer velocities measured at low wind speed over a
1001 lake. *Limnology and Oceanography*, 48(3), 1010–1017.
1002 <https://doi.org/10.4319/lo.2003.48.3.1010>

1003 D’Amario, S.C., & Xenopoulos, M.A. (2015). Linking dissolved carbon dioxide to dissolved
1004 organic matter quality in streams. *Biogeochemistry*, 126(1–2), 99–114.
1005 <https://doi.org/10.1007/s10533-015-0143-y>

1006 Deemer, B.R., Harrison, J.A., Li, S., Beaulieu, J.J., DelSontro, T., Barros, et. al. (2016).
1007 Greenhouse Gas Emissions from Reservoir Water Surfaces: A New Global Synthesis.
1008 *BioScience*, 66(11), 949–964. <https://doi.org/10.1093/biosci/biw117>

1009 Deemer, B.R., & Holgerson, M.A. (2021). Drivers of Methane Flux Differ Between Lakes and
1010 Reservoirs, Complicating Global Upscaling Efforts. *Journal of Geophysical Research:*
1011 *Biogeosciences*, 126(4). <https://doi.org/10.1029/2019JG005600>

1012 DelSontro, T., del Giorgio, P.A., & Prairie, Y.T. (2018). No Longer a Paradox: The Interaction
1013 Between Physical Transport and Biological Processes Explains the Spatial Distribution of
1014 Surface Water Methane Within and Across Lakes. *Ecosystems*, 21(6), 1073–1087.
1015 <https://doi.org/10.1007/s10021-017-0205-1>

1016 Erkkilä, K.M., Ojala, A., Bastviken, D., Biermann, T., Heiskanen, J.J., Lindroth, A., et. al.
1017 (2018). Methane and carbon dioxide fluxes over a lake: Comparison between eddy
1018 covariance, floating chambers and boundary layer method. *Biogeosciences*, 15(2), 429–
1019 445. <https://doi.org/10.5194/bg-15-429-2018>

1020 Esters, L., Rutgersson, A., Nilsson, E., & Sahlée, E. (2021). Non-local Impacts on Eddy-
1021 Covariance Air–Lake CO₂ Fluxes. *Boundary-Layer Meteorology*, 178(2), 283–300.
1022 <https://doi.org/10.1007/s10546-020-00565-2>

1023 Eugster, W. (2003). CO₂ exchange between air and water in an Arctic Alaskan and midlatitude
1024 Swiss lake: Importance of convective mixing. *Journal of Geophysical Research*,
1025 108(D12), 4362. <https://doi.org/10.1029/2002JD002653>

1026 Eugster, W., DelSontro, T., & Sobek, S. (2011). Eddy covariance flux measurements confirm
1027 extreme CH₄; emissions from a Swiss hydropower reservoir and resolve their short-term
1028 variability. *Biogeosciences*, 8(9), 2815–2831. <https://doi.org/10.5194/bg-8-2815-2011>

1029 Gash, J.H.C., & Culf, A.D. (1996). Applying a linear detrend to eddy correlation data in
1030 realtime. *Boundary Layer Meteorology*, 79, 301-306.
1031 <https://doi.org/10.1007/BF00119443>

1032 Gerling, A.B., Munger, Z.W., Doubek, J.P., Hamre, K.D., Gantzer, P.A., Little, J.C., & Carey,
1033 C.C. (2016). Whole-Catchment Manipulations of Internal and External Loading Reveal
1034 the Sensitivity of a Century-Old Reservoir to Hypoxia. *Ecosystems*, 19(3), 555–571.
1035 <https://doi.org/10.1007/s10021-015-9951-0>

1036 Golub, M., Desai, A.R., Vesala, T., Mammarella, I., Ojala, A., Bohrer, G., et. al. (2021). *New*
1037 *insights into diel to interannual variation in carbon dioxide emissions from lakes and*
1038 *reservoirs* [Preprint]. Environmental Sciences. <https://doi.org/10.1002/essoar.10507313.1>

1039 Gómez-Gener, L., Rocher-Ros, G., Battin, T., Cohen, M.J., Dalmagro, H.J., Dinsmore, K.J., et.
1040 al. (2021). Global carbon dioxide efflux from rivers enhanced by high nocturnal
1041 emissions. *Nature Geoscience*, 14(5), 289–294. [https://doi.org/10.1038/s41561-021-](https://doi.org/10.1038/s41561-021-00722-3)
1042 [00722-3](https://doi.org/10.1038/s41561-021-00722-3)

1043 Gorsky, A.L., Lottig, N.R., Stoy, P.C., Desai, A.R., & Dugan, H.A. (2021). The Importance of
1044 Spring Mixing in Evaluating Carbon Dioxide and Methane Flux From a Small North-
1045 Temperate Lake in Wisconsin, United States. *Journal of Geophysical Research:*
1046 *Biogeosciences*, 126(12). <https://doi.org/10.1029/2021JG006537>

1047 Hanson, P.C., Pace, M.L., Carpenter, S.R., Cole, J.J., & Stanley, E.H. (2015). Integrating
1048 Landscape Carbon Cycling: Research Needs for Resolving Organic Carbon Budgets of
1049 Lakes. *Ecosystems*, 18(3), 363–375. <https://doi.org/10.1007/s10021-014-9826-9>

1050 Heiskanen, J.J., Mammarella, I., Haapanala, S., Pumpanen, J., Vesala, T., MacIntyre, S., &
1051 Ojala, A. (2014). Effects of cooling and internal wave motions on gas transfer

1052 coefficients in a boreal lake. *Tellus B: Chemical and Physical Meteorology*, 66(1), 22827.
1053 <https://doi.org/10.3402/tellusb.v66.22827>

1054 Hounshell, A.G. (2022, December 9). aghounshell/EddyFlux: EddyFlux: Hounshell et al. 20XX
1055 re-submission-2 (Version 3.0.0). [Software] Zenodo.
1056 <https://doi.org/10.5281/zenodo.742001>

1057 Howard, D.W., Hounshell, A.G., Lofton, M.E., Woelmer, W.M., Hanson, P.C., & Carey, C.C.
1058 (2021). Variability in fluorescent dissolved organic matter concentrations across diel to
1059 seasonal time scales is driven by water temperature and meteorology in a eutrophic
1060 reservoir. *Aquatic Sciences*, 83(2), 30. <https://doi.org/10.1007/s00027-021-00784-w>

1061 Huotari, J., Ojala, A., Peltomaa, E., Nordbo, A., Launiainen, S., Pumpanen, J., et. al. (2011).
1062 Long-term direct CO₂ flux measurements over a boreal lake: Five years of eddy
1063 covariance data. *Geophysical Research Letters*, 38(18).
1064 <https://doi.org/10.1029/2011GL048753>

1065 Hyndman, R.J. & Athanasopoulos, G. (2018). *Forecasting: principles and practice*, 2nd Edition.
1066 Otexts, Melbourne, Australia.

1067 Hyndman, R., Athanasopoulos, G., Bergmeir, C., Caceres, G., Chhay, L., O'Hara-Wild, M., et al.
1068 (2022, January 10). forecast: Forecasting functions for time series and linear models.
1069 (Version 8.16). [Software]. R Package. <https://pkg.robjhyndman.com/forecast/>

1070 Hyndman, R. J., & Khandakar, Y. (2008). Automatic Time Series Forecasting: The **forecast**
1071 Package for R. *Journal of Statistical Software*, 27(3).
1072 <https://doi.org/10.18637/jss.v027.i03>

1073 Imrit, M.A., & Sharma, S. (2021). Climate Change is Contributing to Faster Rates of Lake Ice
1074 Loss in Lakes Around the Northern Hemisphere. *Journal of Geophysical Research:*
1075 *Biogeosciences*, 126(7). <https://doi.org/10.1029/2020JG006134>

1076 Jammet, M., Crill, P., Dengel, S., & Friborg, T. (2015). Large methane emissions from a
1077 subarctic lake during spring thaw: Mechanisms and landscape significance: Lake

1078 methane emissions among spring thaw. *Journal of Geophysical Research:*
1079 *Biogeosciences*, 120(11), 2289–2305. <https://doi.org/10.1002/2015JG003137>

1080 Jammet, M., Dengel, S., Kettner, E., Parmentier, F.J.W., Wik, M., Crill, P., & Friborg, T. (2017).
1081 Year-round CH₄ and CO₂ flux dynamics in two contrasting freshwater ecosystems of the
1082 subarctic. *Biogeosciences*, 14(22), 5189–5216. <https://doi.org/10.5194/bg-14-5189-2017>

1083 Jonsson, A., Åberg, J., Lindroth, A., & Jansson, M. (2008). Gas transfer rate and CO₂ flux
1084 between an unproductive lake and the atmosphere in northern Sweden: CO₂ emission in
1085 an unproductive lake. *Journal of Geophysical Research: Biogeosciences*, 113(G4).
1086 <https://doi.org/10.1029/2008JG000688>

1087 Klaus, M., Seekell, D.A., Lidberg, W., & Karlsson, J. (2019). Evaluations of Climate and Land
1088 Management Effects on Lake Carbon Cycling Need to Account for Temporal Variability
1089 in CO₂ Concentrations. *Global Biogeochemical Cycles*, 33(3), 243–265.
1090 <https://doi.org/10.1029/2018GB005979>

1091 Kljun, N., Calanca, P., Rotach, M.W., & Schmid, H.P. (2015). A simple two-dimensional
1092 parameterisation for Flux Footprint Prediction (FFP). *Geoscientific Model Development*,
1093 8(11), 3695–3713. <https://doi.org/10.5194/gmd-8-3695-2015>

1094 Kljun, N., Rotach, M.W., & Schmid, H.P. (2002). A Three-Dimensional Backward Lagrangian
1095 Footprint Model For A Wide Range Of Boundary-Layer Stratifications. *Boundary-Layer*
1096 *Meteorology*, 103(2), 205–226. <https://doi.org/10.1023/A:1014556300021>

1097 Lee, X., Massman, W., & Law B. (Eds.). (2005). *Handbook of Micrometeorology A Guide for*
1098 *Surface Flux Measurement and Analysis*, United States of America: Springer Science +
1099 Business Media, Inc.

1100 LiCor Biogeosciences. (2019, December 18). EddyPro® Software (Version 7.0.6) [Software].
1101 LI-COR. <https://www.licor.com/env/support/EddyPro/home.html>

1102 Liu, H., Zhang, Q., Katul, G.G., Cole, J.J., Chapin, F.S., & MacIntyre, S. (2016). Large CO₂
1103 effluxes at night and during synoptic weather events significantly contribute to CO₂

- 1104 emissions from a reservoir. *Environmental Research Letters*, 11(6), 064001.
1105 <https://doi.org/10.1088/1748-9326/11/6/064001>
- 1106 Lofton, M.E. (2022). melofton/FCR-phytos: Lofton et al. 20XX manuscript second revision
1107 (Version 3.0.0.). [Software]. Zenodo. <https://doi.org/10.5281/zenodo.6483433>
- 1108 Loken, L. C., Crawford, J.T., Schramm, P.J., Stadler, P., Desai, A.R., & Stanley, E.H. (2019).
1109 Large Spatial and Temporal Variability of Carbon Dioxide and Methane in a Eutrophic
1110 Lake. *Journal of Geophysical Research: Biogeosciences*, 124(7), 2248–2266.
1111 <https://doi.org/10.1029/2019JG005186>
- 1112 MacIntyre, S., Jonsson, A., Jansson, M., Aberg, J., Turney, D.E., & Miller, S.D. (2010).
1113 Buoyancy flux, turbulence, and the gas transfer coefficient in a stratified lake.
1114 *Geophysical Research Letters*, 37(24). <https://doi.org/10.1029/2010GL044164>
- 1115 Mammarella, I., Nordbo, A., Rannik, Ü., Haapanala, S., Levula, J., Laakso, H., et. al. (2015).
1116 Carbon dioxide and energy fluxes over a small boreal lake in Southern Finland. *Journal*
1117 *of Geophysical Research: Biogeosciences*, 120(7), 1296–1314.
1118 <https://doi.org/10.1002/2014JG002873>
- 1119 Mauder, M., & Foken T. (2006). Impact of post-field data processing on eddy covariance flux
1120 estimates and energy balance closure. *Meteorologische Zeitschrift*, 15, 597-609.
- 1121 McClure, R.P., Hamre, K.D., Niederlehner, B.R., Munger, Z.W., Chen, S., Lofton, M.E.,
1122 Schreiber, M.E., & Carey, C.C. (2018). Metalimnetic oxygen minima alter the vertical
1123 profiles of carbon dioxide and methane in a managed freshwater reservoir. *Science of The*
1124 *Total Environment*, 636, 610–620. <https://doi.org/10.1016/j.scitotenv.2018.04.255>
- 1125 McClure, R.P., Lofton, M.E., Chen S., Krueger, K.M., Little, J.C., & Carey, C.C. (2020). The
1126 Magnitude and Drivers of Methane Ebullition and Diffusion Vary on a Longitudinal
1127 Gradient in a Small Freshwater Reservoir. *Journal of Geophysical Research:*
1128 *Biogeosciences*, 125. <https://doi.org/10.1029/2019JG005205>
- 1129 McClure, R.P., Schreiber, M.E., Lofton, M.E., Chen, S., Krueger, K.M., & Carey, C.C. (2021).
1130 Ecosystem-Scale Oxygen Manipulations Alter Terminal Electron Acceptor Pathways in a

1131 Eutrophic Reservoir. *Ecosystems*, 24(6), 1281–1298. <https://doi.org/10.1007/s10021-020->
1132 [00582-9](https://doi.org/10.1007/s10021-020-00582-9)

1133 McDermitt, D., Burba, G., Xu, L., Anderson, T., Komissarov, A., Riensche, B., et al. (2011). A
1134 new low-power, open-path instrument for measuring methane flux by eddy covariance.
1135 *Applied Physics B*, 102: 391-405. <https://doi.org/10.1007/s00340-010-4307-0>

1136 Moncrieff, J.B., Clement, R., Finnigan, J., Meyers, T. (2004). Averaging, Detrending, and
1137 Filtering of Eddy Covariance Time Series. In: Lee X., Massman W., Law B. (eds)
1138 *Handbook of Micrometeorology*. (Vol 29, pp. 7-31). Springer, Dordrecht.
1139 https://doi.org/10.1007/1-4020-2265-4_2

1140 Moncrieff, J.B., Massheder, J.M., de Bruin, H., Ebers, J., Friborg, T., Heusinkveld, B., et al.
1141 (1997). A system to measure surface fluxes of momentum, sensible heat, water vapor,
1142 and carbon dioxide. *Journal of Hydrology*, 188-189: 598-611.
1143 [https://doi.org/10.1016/S0022-1694\(96\)03194-0](https://doi.org/10.1016/S0022-1694(96)03194-0)

1144 Ouyang, Z., Shao, C., Chu, H., Becker, R., Bridgeman, T., Stepien, C., John, R., & Chen, J.
1145 (2017). The Effect of Algal Blooms on Carbon Emissions in Western Lake Erie: An
1146 Integration of Remote Sensing and Eddy Covariance Measurements. *Remote Sensing*,
1147 9(1), 44. <https://doi.org/10.3390/rs9010044>

1148 Podgrajsek, E., Sahlée, E., Bastviken, D., Holst, J., Lindroth, A., Tranvik, L., & Rutgersson, A.
1149 (2014). Comparison of floating chamber and eddy covariance measurements of lake
1150 greenhouse gas fluxes. *Biogeosciences*, 11(15), 4225–4233. <https://doi.org/10.5194/bg->
1151 [11-4225-2014](https://doi.org/10.5194/bg-11-4225-2014)

1152 Podgrajsek, E., Sahlée, E., Bastviken, D., Natchimuthu, S., Kljun, N., Chmiel, H.E.,
1153 Klemedtsson, L., & Rutgersson, A. (2016). Methane fluxes from a small boreal lake
1154 measured with the eddy covariance method. *Limnology and Oceanography*, 61(S1), S41–
1155 S50. <https://doi.org/10.1002/lno.10245>

- 1156 Prairie, Y.T., Alm, J., Beaulieu, J., Barros, N., Battin, T., Cole, J., et al. (2018). Greenhouse Gas
1157 Emissions from Freshwater Reservoirs: What Does the Atmosphere See? *Ecosystems*,
1158 21(5), 1058–1071. <https://doi.org/10.1007/s10021-017-0198-9>
- 1159 Read, J.S., Hamilton, D.P., Desai, A.R., Rose, K.C., MacIntyre, S., Lenters, J.D., et al. (2012).
1160 Lake-size dependency of wind shear and convection as controls on gas exchange: lake-
1161 size dependency of u^* and w^* . *Geophysical Research Letters*, 39(9).
1162 <https://doi.org/10.1029/2012GL051886>
- 1163 Reed, D.E., Dugan, H.A., Flannery, A.L., & Desai, A.R. (2018). Carbon sink and source
1164 dynamics of a eutrophic deep lake using multiple flux observations over multiple years.
1165 *Limnology and Oceanography Letters*, 3(3), 285–292. <https://doi.org/10.1002/lol2.10075>
- 1166 Rosentreter, J.A., Borges, A.V., Deemer, B.R., Holgerson, M.A., Liu, S., Song, C., et al. (2021).
1167 Half of global methane emissions come from highly variable aquatic ecosystem sources.
1168 *Nature Geoscience*, 14(4), 225–230. <https://doi.org/10.1038/s41561-021-00715-2>
- 1169 Sanches, L.F., Guenet, B., Marinho, C.C., Barros, N., & de Assis Esteves, F. (2019). Global
1170 regulation of methane emission from natural lakes. *Scientific Reports*, 9(1), 255.
1171 <https://doi.org/10.1038/s41598-018-36519-5>
- 1172 Scholz, K., Ejarque, E., Hammerle, A., Kainz, M., Schelker, J., & Wohlfahrt, G. (2021).
1173 Atmospheric CO₂ Exchange of a Small Mountain Lake: Limitations of Eddy Covariance
1174 and Boundary Layer Modeling Methods in Complex Terrain. *Journal of Geophysical*
1175 *Research: Biogeosciences*, 126(7). <https://doi.org/10.1029/2021JG006286>
- 1176 Schubert, C.J., Diem, T., & Eugster, W. (2012). Methane Emissions from a Small Wind Shielded
1177 Lake Determined by Eddy Covariance, Flux Chambers, Anchored Funnels, and
1178 Boundary Model Calculations: A Comparison. *Environmental Science & Technology*,
1179 46(8): 4515-4522. <https://doi.org/10.1021/es203465x>
- 1180 Shao, C., Chen, J., Stepien, C.A., Chu, H., Ouyang, Z., Bridgeman, T.B., Czajkowski, K.P.,
1181 Becker, R.H., & John, R. (2015). Diurnal to annual changes in latent, sensible heat, and
1182 CO₂ fluxes over a Laurentian Great Lake: A case study in Western Lake Erie. *Journal of*

1183 *Geophysical Research: Biogeosciences*, 120(8), 1587–1604.
1184 <https://doi.org/10.1002/2015JG003025>

1185 Sharma, S., Richardson, D.C., Woolway, R.I., Imrit, M.A., Bouffard, D., Blagrove, K., et. al.
1186 (2021). Loss of Ice Cover, Shifting Phenology, and More Extreme Events in Northern
1187 Hemisphere Lakes. *Journal of Geophysical Research: Biogeosciences*, 126(10).
1188 <https://doi.org/10.1029/2021JG006348>

1189 Sieczko, A. K., Duc, N.T., Schenk, J., Pajala, G., Rudberg, D., Sawakuchi, H.O., & Bastviken,
1190 D. (2020). Diel variability of methane emissions from lakes. *Proceedings of the National*
1191 *Academy of Sciences*, 117(35), 21488–21494. <https://doi.org/10.1073/pnas.2006024117>

1192 Smith, S.V., Renwick, W.H., Bartley, J.D., & Buddemeier, R.W. (2002). Distribution and
1193 significance of small, artificial water bodies across the United States landscape. *Science*
1194 *of The Total Environment*, 299(1–3), 21–36. [https://doi.org/10.1016/S0048-](https://doi.org/10.1016/S0048-9697(02)00222-X)
1195 [9697\(02\)00222-X](https://doi.org/10.1016/S0048-9697(02)00222-X)

1196 Sobek, S., Tranvik, L.J., & Cole, J.J. (2005). Temperature independence of carbon dioxide
1197 supersaturation in global lakes: Carbon dioxide supersaturation in global lakes. *Global*
1198 *Biogeochemical Cycles*, 19(2),. <https://doi.org/10.1029/2004GB002264>

1199 Soloviev, A., Donelan, M., Graber, H., Haus, B., & Schlüssel, P. (2007). An approach to
1200 estimation of near-surface turbulence and CO₂ transfer velocity from remote sensing data.
1201 *Journal of Marine Systems*, 66(1–4), 182–194.
1202 <https://doi.org/10.1016/j.jmarsys.2006.03.023>

1203 Taoka, T., Iwata, H., Hirata, R., Takahashi, Y., Miyabara, Y., & Itoh, M. (2020). Environmental
1204 Controls of Diffusive and Ebullitive Methane Emissions at a Subdaily Time Scale in the
1205 Littoral Zone of a Midlatitude Shallow Lake. *Journal of Geophysical Research:*
1206 *Biogeosciences*, 125(9). <https://doi.org/10.1029/2020JG005753>

1207 Tranvik, L.J., Downing, J.A., Cotner, J.B., Loiselle, S.A., Striegl, R.G., Ballatore, T.J., et. al.
1208 (2009). Lakes and reservoirs as regulators of carbon cycling and climate. *Limnology and*
1209 *Oceanography*, 54(6part2), 2298–2314. https://doi.org/10.4319/lo.2009.54.6_part_2.2298

- 1210 USACE (United States Army Corps of Engineers). (2021). National inventory of Dams (NID).
1211 [accessed 2022 February 7]. <https://nid.usace.army.mil/#/>
- 1212 Vachon, D., & Prairie, Y.T. (2013). The ecosystem size and shape dependence of gas transfer
1213 velocity versus wind speed relationships in lakes. *Canadian Journal of Fisheries and*
1214 *Aquatic Sciences*, 70(12), 1757–1764. <https://doi.org/10.1139/cjfas-2013-0241>
- 1215 Vesala, T., Eugster, W., & Ojala, A. (2012). Eddy Covariance Measurements over Lakes. In M.
1216 Aubinet, T. Vesala, & D. Papale (Eds.), *Eddy Covariance* (pp. 365–376). Springer
1217 Netherlands. https://doi.org/10.1007/978-94-007-2351-1_15
- 1218 Vesala, T., Huotari, J., Rannik, Ü., Suni, T., Smolander, S., Sogachev, A., Launiainen, S., &
1219 Ojala, A. (2006). Eddy covariance measurements of carbon exchange and latent and
1220 sensible heat fluxes over a boreal lake for a full open-water period. *Journal of*
1221 *Geophysical Research*, 111(D11), D11101. <https://doi.org/10.1029/2005JD006365>
- 1222 Vickers, D., & Mahrt, L. (1997). Quality Control and Flux Sampling Problems for Tower and
1223 Aircraft Data. *Journal of Atmospheric and Oceanic Technology*, 14(3), 512–526.
1224 [https://doi.org/10.1175/1520-0426\(1997\)014<0512:QCAFSP>2.0.CO;2](https://doi.org/10.1175/1520-0426(1997)014<0512:QCAFSP>2.0.CO;2)
- 1225 Waldo, S., Beaulieu, J.J., Barnett, W., Balz, D. A., Vanni, M.J., Williamson, T., & Walker, J.T.
1226 (2021). Temporal trends in methane emissions from a small eutrophic reservoir: The key
1227 role of a spring burst. *Biogeosciences*, 18(19), 5291–5311. [https://doi.org/10.5194/bg-18-](https://doi.org/10.5194/bg-18-5291-2021)
1228 [5291-2021](https://doi.org/10.5194/bg-18-5291-2021)
- 1229 Wanninkhof, R., Asher, W.E., Ho, D.T., Sweeney, C., & McGillis, W.R. (2009). Advances in
1230 Quantifying Air-Sea Gas Exchange and Environmental Forcing. *Annual Review of*
1231 *Marine Science*, 1: 213-244. <https://doi.org/10.1146/annurev.marine.010908.163742>
- 1232 Watras, C.J., Morrison, K.A., Crawford, J.T., McDonald, C.P., Oliver, S.K., & Hanson, P.C.
1233 (2015). Diel cycles in the fluorescence of dissolved organic matter in dystrophic
1234 Wisconsin seepage lakes: Implications for carbon turnover: Diel CDOM fluorescence
1235 cycles. *Limnology and Oceanography*, 60(2), 482–496. <https://doi.org/10.1002/lno.10026>

- 1236 Webb, E.K., Pearman, G.I., & Leuning R. (1980). Correction of flux measurements for density
1237 effects due to heat and water vapour transfer. *Quarterly Journal of the Royal*
1238 *Meteorological Society*, 106(447), 85-100. <https://doi.org/10.1002/qj.49710644707>
- 1239 Wik, M., Thornton, B.F., Bastviken, D., Uhlbäck, J., & Crill, P.M. (2016). Biased sampling of
1240 methane release from northern lakes: A problem for extrapolation. *Geophysical Research*
1241 *Letters*, 43(3), 1256–1262. <https://doi.org/10.1002/2015GL066501>
- 1242 Wilczak, J.M., Oncley, S.P., Stage, S.A. (2001). Sonic anemometer tilt correction algorithms.
1243 *Boundary-Layer Meteorology*, 99, 127-150. <https://doi.org/10.1023/A:1018966204465>
- 1244 Winslow, L. A., Read, J.S., Hanson, P.C., & Stanley, E.H. (2014). Lake shoreline in the
1245 contiguous United States: Quantity, distribution and sensitivity to observation resolution.
1246 *Freshwater Biology*, 59(2), 213–223. <https://doi.org/10.1111/fwb.12258>
- 1247 Winslow, L., Read, J., Woolway, R., Brentrup, J., Leach T., Zwart, J., Albers, S., & Collinge, C.
1248 (2016a, June 9). LakeAnalyzer: Lake Physics Tools. (Version 1.11.4.1). [Software]. R.
1249 Package. <https://CRAN.R-project.org/package=rLakeAnalyzer>
- 1250 Winslow, L.A., Zwart, J.A., Batt, R.D., Dugan, H.A., Woolway, R.I., Corman, J.R., Hanson,
1251 P.C., & Read, J.S. (2016c). LakeMetabolizer: An R package for estimating lake
1252 metabolism from free-water oxygen using diverse statistical models. *Inland Waters*, 6(4),
1253 622–636. <https://doi.org/10.1080/IW-6.4.883>
- 1254 Winslow, L., Zwart, J., Batt, R., Corman, J., Dugan, H., Hanson, P., et. al. (2016b, June 23).
1255 LakeMetabolizer: Tools for the analysis of ecosystem metabolism. (Version 1.5.0).
1256 [Software]. R Package. <https://CRAN.R-project.org/pacakge=LakeMetabolizer>
- 1257 Woolway, R.I., Kraemer, B.M., Lenters, J.D., Merchant, C.J., O'Reilly, C.M., & Sharma, S.
1258 (2020). Global lake responses to climate change. *Nature Reviews Earth & Environment*,
1259 1(8), 388–403. <https://doi.org/10.1038/s43017-020-0067-5>
- 1260 Wutzler, T., Lucas-Moffat, A., Migliavacca, M., Knauer, J., Sickel, K., Šigut, L., Menzer, O., &
1261 Reichstein, M. (2018). Basic and extensible post-processing of eddy covariance flux data

1262 with REddyProc. *Biogeosciences*, 15(16), 5015–5030. [https://doi.org/10.5194/bg-15-](https://doi.org/10.5194/bg-15-5015-2018)
1263 [5015-2018](https://doi.org/10.5194/bg-15-5015-2018)

1264 Wutzler, T., Reichstein, M., Lucas-Moffat, A.M., Menzer, O., Migliavacca, M., & Sickel, K.
1265 (2021, December 01). REddyProc: Post Processing of (Half-) Hourly Eddy-Covariance
1266 Measurements. (Version 1.3.1). [Software]. R. Package. [https://CRAN.R-](https://CRAN.R-project.org/package=REddyProc)
1267 [project.org/package=REddyProc](https://CRAN.R-project.org/package=REddyProc)